Mechanobiology in Medicine 3 (2025) 100133

Contents lists available at ScienceDirect

Mechanobiology in Medicine

journal homepage: www.sciencedirect.com/journal/mechanobiology-in-medicine

Neuromorphic chips for biomedical engineering☆

Kaiyang Wang[a,b], Shuhui Ren[c], Yunfang Jia[c,*], Xiaobing Yan[d,**], Lizhen Wang[a,b,***], Yubo Fan[a,b,****]

[a] Medical Engineering &Engineering Medicine Innovation Center, Hangzhou International Innovation Institute, Beihang University, 311115, Hangzhou, China
[b] Key Laboratory of Biomechanics and Mechanobiology (Beihang University), Ministry of Education, Beijing Advanced Innovation Center for Biomedical Engineering, School of Biological and Medical Engineering, Beihang University, Beijing, 100191, China
[c] College of Electronic Information and Optical Engineering, Nankai University, Tianjin, 300071, China
[d] Key Laboratory of Brain-Like Neuromorphic Devices and Systems of Hebei Province, Jiaruiyuan Biochip Research Center of Hebei University, College of Electron and Information Engineering, Hebei University, Baoding, 071002, China

ARTICLE INFO

Keywords:
Neuromorphic devices
Biosensing technology
Medical image processing
Rehabilitation medical engineering
Brain-computer interfaces

ABSTRACT

The modern medical field faces two critical challenges: the dramatic increase in data complexity and the explosive growth in data size. Especially in current research, medical diagnostic, and data processing devices relying on traditional computer architecture are increasingly showing limitations when faced with dynamic temporal and spatial processing requirements, as well as high-dimensional data processing tasks. Neuromorphic devices provide a new way for biomedical data processing due to their low energy consumption and high dynamic information processing capabilities. This paper aims to reveal the advantages of neuromorphic devices in biomedical applications. First, this review emphasizes the urgent need of biomedical engineering for diversify clinical diagnostic techniques. Secondly, the feasibility of the application in biomedical engineering is demonstrated by reviewing the historical development of neuromorphic devices from basic modeling to multimodal signal processing. In addition, this paper demonstrates the great potential of neuromorphic chips for application in the fields of biosensing technology, medical image processing and generation, rehabilitation medical engineering, and brain-computer interfaces. Finally, this review provides the pathways for constructing standardized experimental protocols using biocompatible technologies, personalized treatment strategies, and systematic clinical validation. In summary, neuromorphic devices will drive technological innovation in the biomedical field and make significant contributions to life health.

1. Introduction

Biomedical engineering, as a cross-disciplinary subject, has made great development in recent decades, which has greatly contributed to the advancement of the medical and healthcare fields.[1,2] From the development of artificial hearts to the popularization of telemedicine systems, these achievements have not only significantly improved the efficiency of diagnosis and treatment of diseases, but also fundamentally improved people's quality of life.[3,4] In the field of medical sensing, smart wearable devices such as heart rate monitoring bands and blood glucose monitoring patches are becoming an important part of modern health management.[5,6] By integrating high-precision sensors and advanced algorithms, these devices are able to monitor a patient's physiological parameters, such as heart rate, blood pressure, and blood glucose levels, in real-time and accurately. This ability to monitor in real time provides valuable early warning information for doctors and personalized health

☆ Given their roles as editors of this journal, Lizhen Wang and Yubo Fan had no involvement in the peer-review of this article and has no access to information regarding its peer-review. Full responsibility for the peer-review process for this article was delegated to Xiaobo Gong.

* Corresponding authors.
** Corresponding author.
*** Corresponding authors. Innovation Center for Medical Engineering &Engineering Medicine, Hangzhou International Innovation Institute, Beihang University, 311115, Hangzhou, China.
**** Corresponding author. Innovation Center for Medical Engineering &Engineering Medicine, Hangzhou International Innovation Institute, Beihang University, 311115, Hangzhou, China.
E-mail addresses: jiayf@nankai.edu.cn (Y. Jia), yanxiaobing@ime.ac.cn (X. Yan), lizhenwang@buaa.edu.cn (L. Wang), yubofan@buaa.edu.cn (Y. Fan).

https://doi.org/10.1016/j.mbm.2025.100133
Received 28 February 2025; Received in revised form 28 April 2025; Accepted 7 May 2025
Available online 15 May 2025

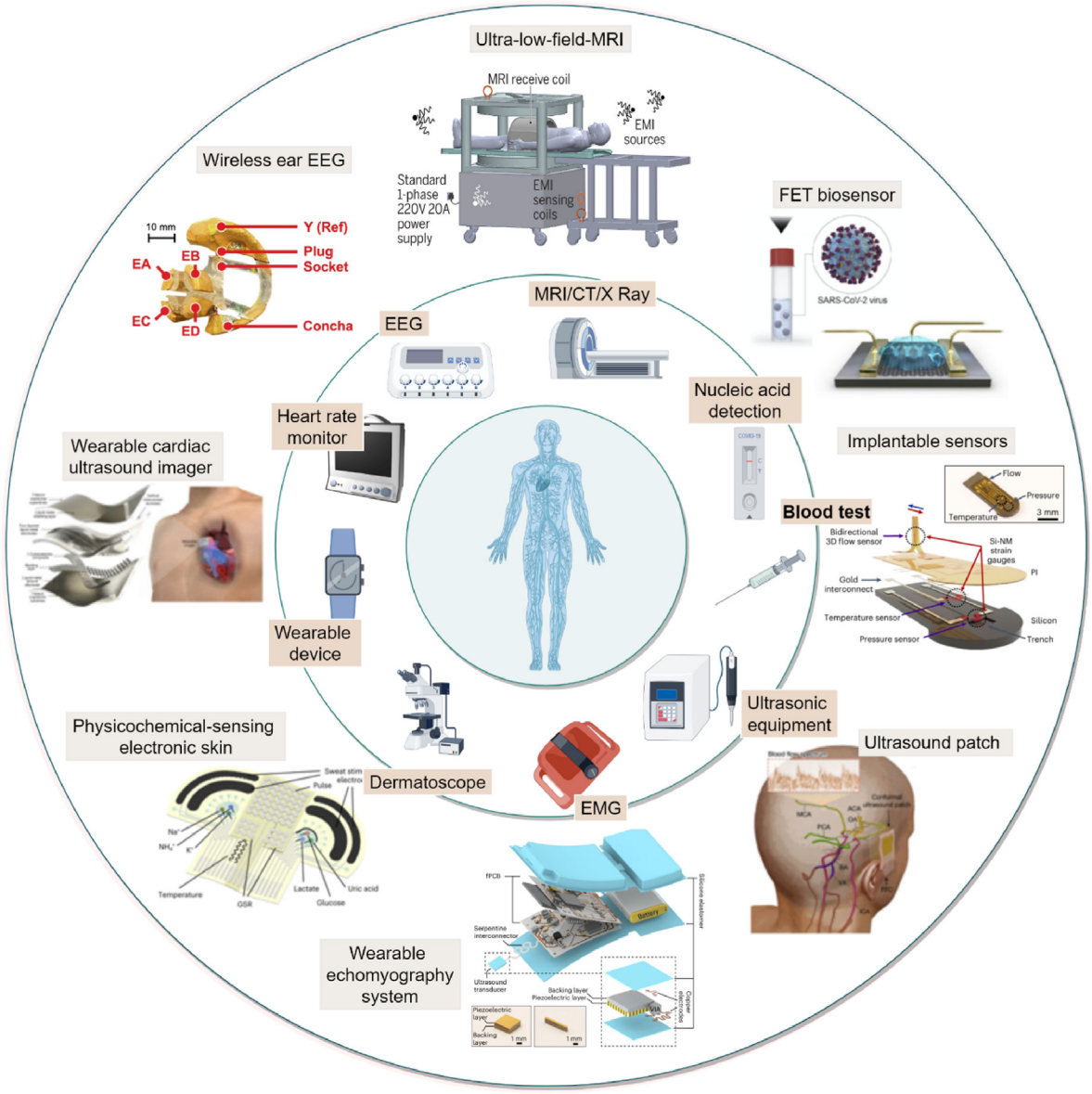

Fig. 1. Schematic diagram of diversify clinical diagnostic techniques for different diseases. Copyright 2024, The American Association for the Advancement of Science.[61] Copyright 2020, American Chemical Society.[62] Copyright 2023, Springer Nature.[63] Copyright 2024, Springer Nature.[64] Copyright 2024, Springer Nature.[65] Copyright 2024, Springer Nature.[66] The figure was drawn by Figdraw.

management programs for patients, thus helping to prevent the onset or progression of disease.[7] In terms of medical image diagnosis, high-resolution medical imaging technologies, such as X-ray,[8,9] magnetic resonance imaging (MRI) and computed tomography (CT),[10,11] provide physicians with a high level of visual insight. These technologies clearly show the body's internal anatomy and functional status, thus helping doctors to more accurately identify and analyze lesions. Combined with advanced image processing algorithms, doctors can further quantify and analyze the imaging data to develop more precise and effective treatment plans.[12,13] However, with the rapid development of the field of biomedical engineering, the challenges it faces are becoming obvious, especially the increase in the complexity and real-time requirements of data processing, which makes the traditional computer architecture gradually expose the limitations. The serial processing of traditional computer architecture is difficult to effectively respond to the parallel computing needs of such massive data. This not only limits the speed of data processing, but also affects the depth and breadth of biomedical research.[14,15] Therefore, exploring new smart chips, especially neuromorphic chips with highly parallel processing capability, has become a key path to solve this challenging problem. Neuromorphic chips mimic the workings of neurons in the human brain and are capable of realizing highly efficient parallel computation, thus dramatically increasing the speed and efficiency of data processing.[16,17] Such chips have great potential for application in the biomedical field and are expected to provide strong technical support for early diagnosis of diseases, precise treatment, and health management.

In recent years, neuromorphic chips have seen significant development at both the device and architectural levels, encompassing cutting-edge technologies such as memristor-based neuromorphic systems,[18,19] convolutional neural network (CNN) chips,[20,21] and application-specific integrated circuits (ASICs) specifically designed to simulate neuronal and synaptic functions.[22,23] By simulating the operation principle of biological neural networks, these devices have successfully broken through the inherent limitations of traditional computer architectures in handling complex parallel tasks, and have demonstrated higher energy-efficiency ratios and lower power consumption in handling complex tasks, which

will provide strong support for the development of future intelligent devices. In particular, it excels in integration and algorithm acceleration. At the integration level, neuromorphic chips, with their highly integrated neuronal and synaptic network architectures, are able to deal with neural computation challenges, thereby significantly reducing system power consumption.[24,25] In terms of algorithm acceleration, these chips are able to efficiently execute complex algorithms such as deep learning and reinforcement learning with the help of bio-inspired advanced learning mechanisms, such as Spike Timing Dependent Plasticity (STDP), which dramatically improves computational speed and accuracy.[26,27] For example, Wu et al. developed an all-hardware convolutional neural network (CNN) neuromorphic chip based on memristors.[21] This chip integrated 8 arrays, each containing 2048 memristors, and successfully constructed a five-layer CNN. It demonstrates excellent image recognition capability under low power consumption conditions. achieving a recognition accuracy of over 96 %. This achievement not only breaks the bottleneck of the traditional von Neumann architecture to a certain extent but also realizes a significant increase in arithmetic power and a significant reduction in power consumption and hardware cost. In addition, Goswami et al. reported a molecular memristor cross-switching matrix that can be integrated into CMOS circuits.[28] This matrix exhibits 14-bit analog accuracy, near-perfect linear and symmetric weight updating properties, and offers one-step programmability at each conductance level. In particular, it reduces energy consumption by a factor of 460 compared to conventional electronic computers. Given the numerous advantages of neuromorphic chips, an increasing number of researchers are actively exploring their potential for biomedical applications to address the complex problems faced in this field.

The purpose of this review is to explore the potential of neuromorphic chips in biomedical applications. First, the urgent need of biomedical engineering for diversified technologies is highlighted based on clinical diagnostic techniques for various parts of the human body and related diseases, including the central nervous system, heart conditions, lung disorders, bone issues, skin problems, muscle conditions, immune system disorders, and viral infections. Second, the feasibility of applying neuromorphic chips in biomedical engineering is demonstrated through a systematic and comprehensive literature survey on the development of neuromorphic devices from basic modelling to multimodal signal processing, as well as mainstream applications in biomedicine. Thirdly, the high-precision, parallel processing, and powerful human-computer interaction capabilities of neuromorphic devices, when applied in biomedical engineering, are demonstrated through specific practical solutions in four mainstream application areas: biomedical sensing technology, medical image processing and generation, rehabilitation medical engineering, and brain-computer interfaces. Finally, the challenges and future trends of neuromorphic devices in biomedical engineering are outlined, including biocompatible technologies, personalized therapeutic strategies and systematic clinical validation, to provide scientific guidance for the clinical application of neuromorphic chips in biomedical engineering.

2. Diversified needs for disease diagnosis

2.1. Central nervous system diseases

Central nervous system (CNS) diseases, as a major category of diseases affecting human health and quality of life, cover a wide area from the brain to the spinal cord, and their causes are complex and diverse, involving genetics, environment, trauma, and other aspects.[29,30] These causes interact with each other, leading to abnormalities in the structure and function of the central nervous system, which in turn lead to a series of clinical symptoms.[31,32] For example, epilepsy (Fig. 1), a chronic neurological disorder, is mainly caused by abnormal discharges of neurons in the brain.[33] Genetic factors play an important role in the development of epilepsy, with some types of epilepsy having a familial predisposition.[34] In addition, head injury, metabolic disorders and abnormal brain function are also important causes of epilepsy.[35,36] In terms of testing methods, Electroencephalogram (EEG) is the tool of choice for evaluating the functional state of the brain and abnormal discharges, which can aid in the diagnosis of epilepsy.[37,38] Meanwhile, imaging tests such as cranial magnetic resonance imaging (MRI) and computed tomography (CT) can also provide detailed structural information about brain tissue, which can help to identify the underlying causes of epilepsy.[39,40] Parkinson's disease, a degenerative disorder of the central nervous system commonly observed in the elderly, is characterized by symptoms such as slowed movement and postural instability.[41,42] As individuals age, the aging of the nervous system and neuronal degenerative changes become important factors contributing to the onset of Parkinson's.[43] In terms of diagnostic methods, a physical examination is typically employed to initially assess motor function and coordination. Kaveh et al. proposed a novel wireless ear EEG sensor fabrication method that was integrated with an existing wireless data collection platform and validated on 9 subjects using an machine learning classification method. The experimental results show an accuracy of 93.3 % in evaluating never-before-seen users using the optimal model of Support Vector Machines. The application of this system and its offline classifier lays the foundation for future covert, completely wireless, long-term, longitudinal brain monitoring.[44] However, conventional computing architectures face high energy consumption and low energy efficiency bottlenecks due to the separate memory-computing design, and have inherent limitations in processing high-dimensional neural signals and integrating multimodal data. These limitations make EEG abnormalities not fully consistent with clinical manifestations, which hampers the diagnostic accuracy and therapeutic efficacy of CNS disorders. The integrated memory-computer architecture of neuromorphic chips provides an obvious advantage for parallel processing of multidimensional biological data, and provides a physical carrier for constructing a new computing paradigm adapted to the complex information processing mechanism of the human brain. Such capabilities are critical for resolving inconsistencies between EEG abnormalities and clinical symptoms, thereby improving diagnostic accuracy for epilepsy and other CNS disorders.

2.2. Heart disease

Heart diseases, such as congenital heart disease and hypertrophic cardiomyopathy, exhibit obvious familial aggregation, as shown in Figs. 1.[45,46] Additionally, poor living habits, including smoking,[47] excessive alcohol consumption,[48] and fat,[49] are also significant triggers of heart diseases. Immunological diseases such as rheumatic heart disease and myocarditis are caused by the immune system mistakenly attacking its own tissues,[50] leading to destruction of heart valves and damage to cardiac muscle cells, thereby causing heart diseases. Electrocardiogram (ECG),[51] as a non-invasive, convenient, and sensitive test for detecting heart diseases, reflects the electrophysiological state of the heart by recording the weak electrical signals generated by cardiac activity, thereby assessing the function and rhythm of the heart. For heart diseases such as arrhythmia, myocardial ischemia, and myocardial infarction, ECG is able to capture abnormal electrical signals and provide direct evidence for diagnosis. Some doctors also use palpation to feel and detect the pulse beat by pressing directly on the radial artery.[52] Meanwhile, increasing numbers of people are focusing on adopting portable pulse diagnostic devices or functional watches. These devices capture pulse information through sensors and convert it into digital signals for pulse measurement, data recording, and analysis, thus reflecting the health status of the heart.[53] Hu et al. report a wearable cardiac ultrasound imager that improves the mechanical coupling between the device and human skin through innovations in design and material fabrication, allowing the left ventricle to be examined from different perspectives during exercise. The study also developed a deep learning model that automatically extracts left ventricular volumes from continuous image recordings, generating waveforms of key cardiac performance metrics such as heartbeats, cardiac output, and ejection fraction. The technology

enables dynamic wearable monitoring of cardiac performance in a variety of environments, significantly enhancing the accuracy of monitoring.[54] Nevertheless, the dynamic nature of cardiac electrical activity and inter-individual variability demand computational systems capable of adaptive learning. Neuromorphic chips, with their ultra-low power consumption and temporal signal processing capabilities, are uniquely suited to decode personalized cardiac electrophysiological patterns from continuous ECG/ultrasound data streams. This technology could enable real-time detection of transient arrhythmias that conventional methods might miss, while reducing the computational burden of deep learning models.

2.3. Lung disease

The causes of lung diseases are closely related to infections. In clinical practice, bacterial pneumonia, caused by Streptococcus pneumoniae and *Staphylococcus aureus*, is the most common type.[55,56] On the other hand, viral pneumonia is most commonly seen in infections caused by viruses like influenza virus and adenovirus.[57] Besides infectious factors, physical and chemical factors are also important causes of lung diseases.[58] Prolonged exposure to harmful chemicals, fumes, dust, etc. can cause damage to lung tissues and increase the risk of developing lung diseases. These physical and chemical factors can directly cause irritation and damage to lung tissue, disrupting the barrier function of the respiratory tract and increasing the risk of pathogen infection. Imaging techniques play a crucial role in the detection of lung diseases. One of the first choices for the diagnosis of lung diseases is CT,[59] which clearly shows the structure of the lungs and has a high sensitivity and specificity for detecting inflammation, tumors, nodules, and other lesions, as shown in Fig. 1. MRI can clearly show the soft tissue structure of the lungs,[60] which is important for determining whether a lung tumour has invaded blood vessels, nerves, and other structures in the mediastinum. In addition, ultrasound imaging can scan human organs using ultrasound probes that emit ultrasound beams. As these beams propagate inside human tissues, they generate reflection and scattering phenomena. The reflected ultrasound signals are then received by the probe, and after transmission, amplification, and processing, an image is formed and displayed on the screen. However, since the lungs contain a large amount of air, this air appears as a low signal on MRI images, affecting the observation of the lungs' fine structures. This fundamental physical limitation demands innovative computational approaches for pulmonary image reconstruction. Neuromorphic chips with in-memory computing capabilities can implement compressed sensing algorithms directly at the sensor interface, reconstructing high-fidelity lung MRI images.

2.4. Bone disease

Fractures, i.e., disruption of the integrity of the bone, are usually caused by external forces acting on the bone, such as falls, traffic accidents, and sports injuries.[67] These external forces may act directly on the bone, causing it to break, or they may cause the bone to fracture at a site remote from the point of action of the force, through conduction or leverage. In addition, osteoporosis is an important cause of fractures in the elderly.[68] As bone density gradually decreases with age, bones become fragile and brittle, and the slightest external force may lead to fractures. Furthermore, Imaging technology plays a pivotal role in the detection of fractures and orthopaedic diseases. X-ray is one of the most commonly used methods of fracture detection.[69] It can clearly show the morphology, structure, and position of the bones, helping doctors to determine whether there is a fracture, as well as the type and extent of the fracture. For complex fractures or fractures involving joints, CT scanning provides more detailed information. CT can generate three-dimensional images and observe the details of the fracture from multiple angles, including the direction of the fracture line and the displacement of the fracture block, which provides important reference for doctors in formulating a surgical plan.[70] MRI is also widely used in the diagnosis of orthopaedic diseases, and has unique advantages in assessing soft tissue injuries.[71] In addition, MRI can detect bone marrow oedema, bone contusion, and other lesions that are not easily visible on X-rays and CTs, providing strong support for early diagnosis and treatment. Wu et al. developed a highly simplified ultra-low-field whole-body MRI scanner using a compact 0.05 T permanent magnet, incorporating active sensing and deep learning techniques to address electromagnetic interference. Healthy volunteers were imaged, and images of the brain, spine, abdomen, lungs, musculoskeletal system, and heart were obtained. Imaging of these organs and structures in healthy volunteers was achieved. In addition, the deep learning-based image formation method effectively suppressed noise and artifacts, improved image spatial resolution, and significantly enhanced the quality of 0.05 T MRI images when imaging the brain, spine, abdomen, and knee. These findings are expected to pave the way for the realization of low-cost, patient-centered, deep learning-driven ultra-low-field MRI scanners.[61] However, to meet the demand for better image quality and higher imaging speeds, the number of MRI radiofrequency coils and CT detectors has increased dramatically, leading to an explosive growth in raw data to be processed. Against the backdrop of slowing Moore's Law driven scaling, such computationally intensive tasks pose severe challenges to traditional von Neumann architecture - based computing hardware, which in turn limits its energy efficiency. Consequently, the speed and energy consumption of image reconstruction have become critical bottlenecks in the development of portable medical imaging systems. Fortunately, the computing-in-memory technology of neuromorphic devices can provide an ultra-efficient alternative solution for medical image reconstruction, breaking the von Neumann bottleneck. In this paradigm, computations are performed where data is stored, governed by physical laws, thereby significantly reducing energy intensive data movement.

2.5. Skin diseases

Infectious skin diseases are the most common type of skin diseases, mainly caused by microbial infections such as bacteria, fungi, and viruses.[72] For example, folliculitis and boils are usually caused by bacterial infections like *Staphylococcus aureus* and (possibly) Streptococcus pyogenes in bacterial skin diseases. Allergic skin diseases,[73] such as eczema and urticaria, are mainly caused by the patient's abnormal immune response to certain substances. Allergens may include food, medication, pollen, dust mites, and other similar substances.[74,75] Furthermore, when patients come into contact with these allergens, symptoms such as redness and itching of the skin will promptly appear. Moving on to diseases, those with abnormalities of the immune system, like psoriasis and lupus erythematosus, usually exhibit family clusters.[76] Notably, the immune system plays a pivotal role in their development. Moreover, physical or chemical factors, such as sunlight,[77] can directly cause skin damage. These external influences further illustrate the complexity and sensitivity of our skin. Dermatoscope is a non-invasive method of skin examination that clearly shows the fine structure and lesions on the skin surface through high magnification and illumination with a special light source.[78] Skin tissue biopsy, on the other hand, is an invasive examination method typically used for diagnosing suspected infections, tumors, and other diseases.[79] This method is particularly important for diagnosing challenging skin conditions such as skin cancer and lupus erythematosus. It involves various procedures, including eosinophil count and IgE level measurement, which can aid in the diagnosis of skin diseases related to the immune system. Xu et al. report an e-skin for stress response that noninvasively monitors three vital signs (pulse waveform, skin current response, and skin temperature) and six molecular biomarkers (glucose, lactate, uric acid, sodium ion, potassium ion, and ammonium) in human sweat. The e-skin provides continuous multimodal physicochemical monitoring over a 24-h period and during different daily activities. With the help of a machine learning pipeline, the platform can differentiate between the three stressors with 98.0 % accuracy and quantify the psychological stress response with 98.7 % confidence,

enabling long-term, continuous stress monitoring.[66] In practical applications, doctors will select the appropriate examination method based on the patient's specific situation and clinical manifestations, in order to achieve an accurate diagnosis and effective treatment. These traditional diagnostic approaches find it challenging to correlate these heterogeneous datasets (such as biomarkers, pulse waveforms, and temperature) in real time. Neuromorphic computing architectures, with their inherent capability to process sparse, event - based sensor data, could facilitate on - device fusion of multimodal dermatological signals. This offers a promising avenue for achieving accurate diagnosis and effective treatment.

2.6. Muscle diseases

Myasthenia gravis is a complex autoimmune disease that primarily affects the transmission function at the neuromuscular junction, resulting in muscle weakness.[80] Prolonged physical or mental overexertion, along with sleep deprivation, may lead to a decrease in the body's immunity, potentially triggering myasthenia gravis.[81] This occurs because overexertion impacts the transmission function at the neuromuscular junction, causing damage to acetylcholine receptors. Abnormalities within the autoimmune system represent a common and significant cause of myasthenia gravis. The patient's body produces antibodies against the acetylcholine receptor, which bind to the receptor and disrupt normal signaling at the neuromuscular junction, leading to weak muscle contractions.[82] In diagnosing myasthenia gravis, repetitive nerve stimulation via electromyography, which observes abnormalities between nerve conduction and muscle contraction, serves as an important tool to confirm the diagnosis.[83] Recently, Gao et al. reported a fully integrated wearable acoustic electromyography (EMG) system, consisting of a customized transducer, a wireless circuit for data processing, and an on-board battery for power supply. The system can be attached to the skin to provide accurate, long-term wireless monitoring of muscles. It is used to detect diaphragm activity, enabling the recognition of different breathing patterns. The authors also developed a deep learning algorithm to correlate single-transducer RF data from forearm muscles with hand gestures, accurately and consistently tracking 13 hand joints with an average error of only 7.9°. This result demonstrates the potential of wearable EMG systems for applications in health monitoring and human-computer interaction.[65] Additionally, an acetylcholine receptor antibody test is employed to ascertain whether an antibody-mediated immune response is occurring and to detect the onset of myasthenia gravis.[84] While electromyography and acetylcholine receptor antibody testing are crucial in diagnosing myasthenia gravis, the causes of the disease are complex and multifaceted, and each diagnostic method has its inherent limitations. The complex temporal dynamics of neuromuscular signals require specialized processing beyond conventional digital signal processing techniques. Neuromorphic chips implementing spiking neural networks can directly process raw EMG spikes with nanosecond temporal precision, enabling real-time detection of myasthenic crisis precursors through synaptic plasticity-based learning mechanisms.

2.7. Immune diseases

Immune system disorders are complex and varied, associated with abnormal activation or dysfunction of the immune system.[85] This results in the body's ability to mount an attack response against its own tissues or fail to fight off external pathogens effectively. Normally, the body's immune system recognizes and eliminates foreign pathogens while avoiding an immune response to its own tissues.[86] However, in some cases, the immune system becomes disordered, mistakenly identifying its own tissues as foreign and initiating an attack, leading to the production of autoimmune antibodies that cause tissue damage and disease. Blood tests are one of the commonly used and crucial tools in detecting immune system disorders.[87] Routine blood tests, C-reactive protein tests, immunoglobulin measurements, lymphocyte counts, and classification tests, among others, can assess the immune function status of the body, aiding in the diagnosis of immune system diseases. Besides blood tests, cellular imaging technology also plays a significant role in detecting immune system diseases.[88] This technique allows for the observation of the morphology, distribution, and functional status of immune cells, providing vital information for the diagnosis and treatment of immune system disorders. However, the temporal and spatial heterogeneity and nonlinear dynamic regulation exhibited by immune response systems pose a serious challenge to traditional computational architectures. For example, T lymphocyte mediated adaptive immune response involves multi - scale signal integration. The ultrafast temporal resolution and micrometer level spatial localization accuracy of this process require computing platforms with dynamic response capabilities adapted to biological speed. In this context, neuromorphic chips show unique advantages: their event driven information processing mechanism can accurately simulate the formation process of immune response. By constructing antibody functionalized interfaces based on memristor, this kind of biomimetic computation not only realizes the dynamic simulation of the T cell receptor signaling pathway with nanojoule energy consumption but also simulates the behavior of T cells through synaptic plasticity, providing a hardware foundation for the construction of a digital immune system with autonomous learning capabilities.

2.8. Viral diseases

Viruses are an extremely diverse group of microorganisms that invade the human body through different modes of transmission, such as respiratory tract infections, gastrointestinal tract infections, blood transfusions, mother-to-child transmission, direct contact, and insect and mosquito bites.[89] For example, influenza viruses and neo-coronaviruses are mainly transmitted through the respiratory tract,[90] while noroviruses and rotaviruses are mainly transmitted through the digestive tract.[91] Nucleic acid tests and blood tests play a crucial role in the detection of viral diseases. The nucleic acid test is one of the most important means of diagnosing viral diseases today.[92] It uses molecular biology techniques such as polymerase chain reaction (PCR) to amplify and detect viral nucleic acids (DNA or RNA) to determine the presence of viral infection. This test is highly sensitive and specific, and is capable of detecting very small amounts of the virus. Blood tests are also important in the detection of viral diseases. Through routine blood tests,[93] changes in the number of blood cells and their morphological distribution can be observed, thus determining the condition of the blood and the disease. Seo et al. reported a field-effect transistor (FET)-based biosensing device for detecting the SARS-CoV-2 virus in clinical samples. The study demonstrated that the prepared FET device could detect the severe acute respiratory syndrome coronavirus 2 (SARS-CoV-2) spiking protein at a concentration of 1 fg/mL in phosphate-buffered saline and 100 fg/mL in clinical transfer medium. Consequently, the authors successfully fabricated a promising FET biosensor for SARS-CoV-2 detection.[62] However, the detection of viral diseases also faces a number of challenges. First, the diversity of viruses complicates detection. Different types of viruses require different detection methods and reagents, which increases the difficulty and cost of detection. Second, the sensitivity and specificity of detection methods need to be balanced. Too much sensitivity may lead to false positive results. To overcome these challenges, the medical community is constantly striving to improve and refine viral disease detection methods, develop new detection techniques and reagents, and increase the sensitivity and specificity of detection. Neuromorphic biosensors, grounded in their biomimetic analog computing architecture, spearhead a revolutionary paradigm in biosensing technology. By mimicking the neural pulse coding mechanisms and event driven attributes of biological nervous systems, this cutting-edge innovation facilitates highly precise antigen antibody detection directly at the device hardware level, yielding substantial enhancements in real-time responsiveness and energy conservation. The integrated reservoir computing architecture further presents a novel approach for ultra-precise detection. This hardware

algorithm co-design philosophy completely reshapes traditional passive detection into an intelligent, proactive monitoring system with predictive prowess, paving the way for promising new technological strategies in early epidemic alert and disease prevention.

It is evident that the modern medical field faces two critical challenges: the dramatic increase in data complexity and the explosive growth in data size. These challenges not only elevate the complexity of disease diagnosis but also set stringent standards on traditional diagnostic methods. Especially in current research, medical diagnostic and data processing devices relying on traditional computer architecture are increasingly showing limitations when dealing with flexible and dynamic temporal and spatial demands, as well as high-dimensional data processing tasks. This, in turn, hinders the enhancement of diagnostic efficiency. Therefore, innovating artificial intelligence technology and developing new electronic devices to create diversified solutions, such as high-performance biosensing technology, medical image analysis, rehabilitation medical equipment, and brain-computer interface technology, has become the pivotal path to improving diagnostic accuracy and efficiency. Neuromorphic chips address these dual challenges through their fundamental architectural advantages: Event driven computation eliminates redundant data processing in time varying biomedical signals, thus reducing power consumption compared to von Neumann architectures; Massively parallel analog processing enables real time analysis of high dimensional medical images (CT/MRI) by means of in memory computing, thereby bypassing the memory wall limitation. By integrating these chips with AI systems, we can achieve closed loop diagnostic platforms that continuously adapt to patient - specific pathophysiological patterns.

3. Neuromorphic device

Neuromorphic devices, which integrate sensing, storage, and computation functions, can achieve highly sensitive detection of biomolecules, as well as storage and computation of the detection data by means of high speed, low energy consumption, and parallel data processing. This innovative technology opens up new development paths in the field of biomedical engineering.[94,95] Neuromorphic device, which is mainly composed of electrodes and a functional layer, is a new type of electronic device that simulates a biological synapse.[96] The electrodes at the two ends of the functional layer can be analogous to the presynaptic and postsynaptic membranes in a biological synapse. The electrical signal conduction and regulation characteristics of these electrodes are highly similar to those of neural signal transmission in a biological synapse, enabling the artificial synaptic device to effectively simulate biological neural signal transmission. From the perspective of device structure, current neuromorphic devices are mainly divided into two types: synaptic transistors and memristors, as shown in Fig. 2. Memristors excel in high-density integration and non-volatile memory capabilities, making them ideal for parallel computing. However, their switching endurance and cycle-to-cycle variability pose challenges for long-term stability. Synaptic transistors, on the other hand, offer precise analog modulation of synaptic weights through gate voltage control and demonstrate superior CMOS compatibility, though they are constrained by Moore's Law compared to memristors. Ultimately, the choice between these two architectures often depends on specific application requirements: memristors are favored for memory-centric neuromorphic systems, while synaptic transistors are preferred for scenarios demanding dynamic synaptic plasticity emulation. Below is a brief description of their typical structures and their applications.

3.1. Memristor

Memristors have a 'sandwich' structure consisting of a top electrode, a functional layer, and a bottom electrode. The resistance value of memristors is regulated by current signals and they possess a memory function.

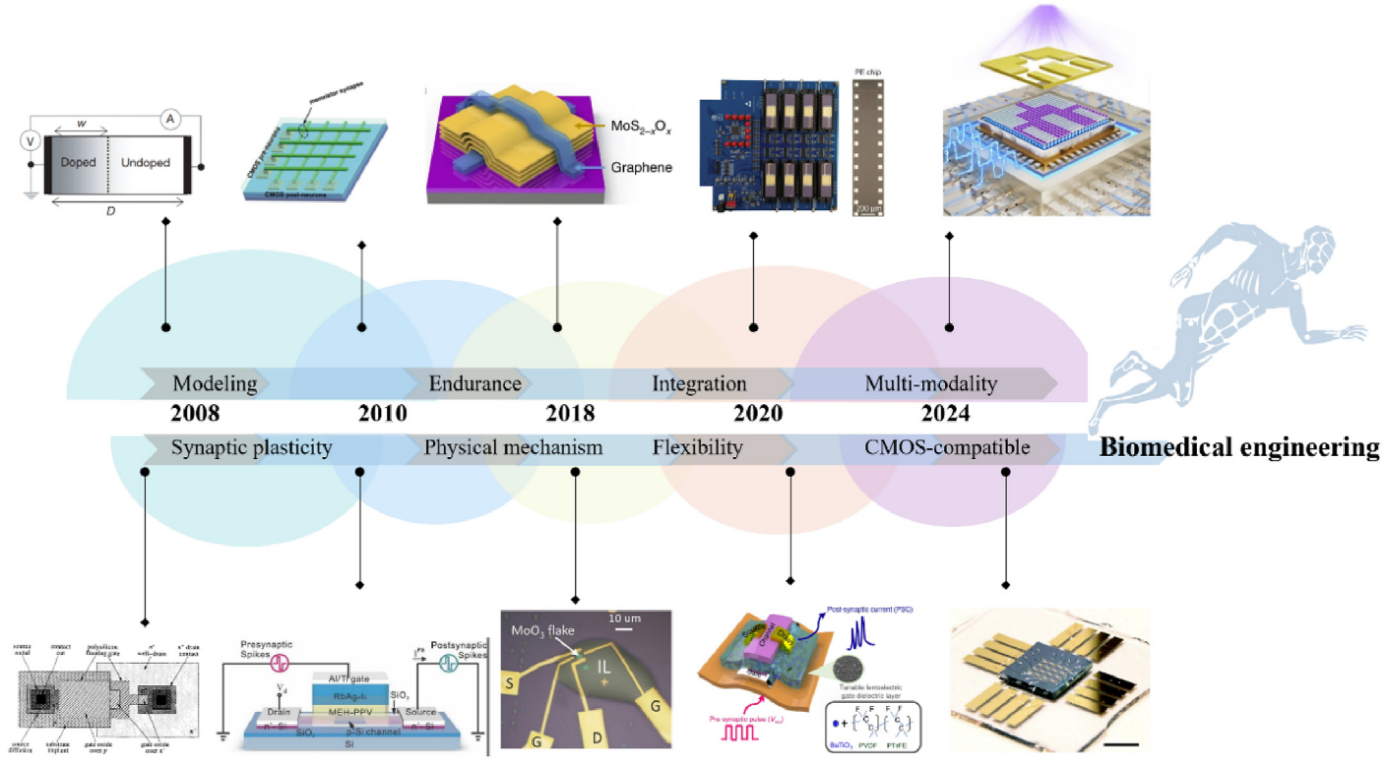

Fig. 2. Historical development of neuromorphic chips. Memristor model. Memristor crossbar. 2D materials based memristor. Fully hardware-integrated memory-computing system. Photo-memristor chip. Synaptic transistor model. Ionic/electronic hybrid synaptic transistor. 2D materials based synaptic transistor. Flexible organic field-effect synaptic transistor. Synaptic transistor array. Copyright 2008, Springer Nature.[97] Copyright 2010, American Chemical Society.[98] Copyright 2024, Springer Nature.[100] Copyright 1996, IEEE.[101] Copyright 2010, WILEY-VCH Verlag GmbH & Co. KGaA, Weinheim.[102] Copyright 2017, WILEY-VCH Verlag GmbH & Co. KGaA, Weinheim.[103] Copyright 2023, Springer Nature.[104].

In 2008, HP published an article in Nature proving the existence of memristors.[97] In 2009, the company further proved that memristors can be formed into interlocking stacks through the Crosslantch system, and demonstrated that the theoretical speed of operation is much higher than that of DRAM. Additionally, the lattice-like design of the structure exhibits a high degree of logical coherence. This represents a theoretical coexistence of computing and memory functions, formally demonstrating the potential of memristors to serve as brain-like chips. Furthermore, scientists at Hewlett-Packard Labs concluded in their research that Resistance-Revolutionary Memory (RRAM) was indeed the memristor and provided the original theoretical foundation for it. From then on, research on memristors gradually gained momentum and flourished. In 2010, Lu et al. presented a nanosilicon-based memristor, and demonstrated that a hybrid system consisting of a CMOS device and a memristor could accomplish the simulation of the basic properties of neural synapses, such as Spike-Timing Dependent Plasticity (STDP).[98] In this experiment, the memristor was used as a synapse mimicking device in neuromorphic circuits, providing an efficient computational approach and high density. Wang et al. report a van der Waals heterojunction memristor that utilizes two-dimensional layered molybdenum disulfide (MoS_2), as well as graphene, to form a sandwich structure.[99] Test results indicate that this fully 2D material-based heterojunction exhibits extremely stable switching behavior, including over ten million (10^7) erasable cycles, an erasure rate of less than 100 ns, and excellent non-volatility. The structure is capable of stable operation at temperatures up to 340 °C and maintains good switching performance, marking an important step forward in promoting the application of memristors in high-temperature electronics and related technologies. Wu et al. have built a fully hardware-integrated memory-computing system utilizing multi-array memristor technology.[21] This system not only achieves architectural innovation but also successfully deploys and efficiently runs convolutional neural network algorithms on its platform. This breakthrough not only validates the superior performance of the system in image recognition tasks but also achieves a significant two-order-of-magnitude improvement in energy efficiency compared to traditional graphics processor chips. This achievement signifies that, through their innovative design, computing devices are able to significantly reduce power consumption and hardware costs while substantially increasing computing power, thereby providing a more efficient and cost-effective solution for complex computing tasks.

In 2024, Huang et al. reported a novel double-layer oxide photomemristor featuring a Pd/TiOx/ZnO/TiN structure, in which a TiO_x interfacial layer was introduced to enhance the stability of the resistive switching and to improve the photoelectric response.[100] Furthermore, the research team successfully integrated a 128 × 8 array comprising 1024 1T-1OEM photoelectric memristor units onto the top of a silicon-based CMOS decoder circuit, utilizing a CMOS back-channel compatibility process. Through photoelectric testing, they verified that the array exhibits good uniformity and stability, and simultaneously, it can realize the integration of multibit programming and sense-storage-calculation functions. For the first time, an all-optical memristor-based reserve pool computing system has been constructed. This system consists of 18 D-OEM mode devices forming the reserve pool layer and 1024 × 5 EM mode devices comprising the readout layer. It achieves an accuracy of 91.2 % with very low energy consumption in the human motion recognition task, thereby providing a high-efficiency hardware platform for intelligent vision applications in complex scenes. The key advantages of memristors lie in their nanoscale scalability, ultra-low power consumption, and ability to simultaneously store and process data. Nevertheless, challenges persist in achieving uniform resistive switching across large arrays, ensuring low leakage current, and mitigating sneak current paths in crossbar architectures.

3.2. Synaptic transistor

The synaptic transistor shares a similar basic structure with the traditional field-effect transistor.[105] It mainly consists of a functional layer, as well as a metal gate, source, and drain. The signal connection strength between the source and drain can be altered by adjusting the gate voltage, thereby simulating synaptic plasticity behavior. Compared to memristors, synaptic transistors generally show better linearity in weight updates but face trade-offs in power efficiency during analog operation. A plethora of research results indicate that synaptic transistors exhibit great potential and advantages in large-scale preparation, long-term data storage, and neural network computation.[106] Diorio et al. have developed a novel floating-gate silicon MOS transistor specifically for analogue learning applications.[101] They have derived a memory-update rule based on the physics of tunneling and injection processes, and have investigated synapse learning in a prototype. Unlike conventional EEPROM devices, the synaptic devices they prepared allow simultaneous memory reads and writes. This lays the foundation for the development of dense, low-power silicon-based learning systems. Chen et al. designed and fabricated a synaptic transistor based on an ionic/electronic hybrid material by integrating a layer of ionic conductor and a layer of ion-doped conjugated polymer onto the gate of a silicon-based transistor.[102] The device is capable of generating EPSCs at intervals of a few milliseconds and achieving synaptic plasticity behaviors, such as STDP, by varying the pulse width and interval of the pulse train. This provides a novel approach to constructing neuromorphic circuits that closely mimic the nerves and functions of the brain. Sun et al. prepared a three-terminal resistive change device, utilizing a thin single-crystal sheet of the two-dimensional material α-MoO_3 as the channel material.[103] By employing an ionic liquid as the gate and applying an electric field to inject hydrogen ions into the interstitial layer of the 2D material, the polymorphic reversible change in the resistance of the α-MoO_3 channel was achieved under low-energy conditions. Furthermore, behaviors such as neural synaptic weight enhancement, inhibition, and the transition from short-term to long-term memory were successfully simulated using the changes in the resistive states of the device. This work demonstrates the feasibility of utilizing solid-state electrochemical processes in the two-dimensional material α-MoO_3 to simulate neural synaptic behaviors. It also provides a technological reference for the development of neural synaptic-like transistors and memory devices with low-power consumption and good scalability, enabling the construction of highly efficient neural network computers. Inspired by the structure of the Merkel cell-axon complex, Lee et al. developed a bionic afferent neural device utilizing a flexible organic field-effect synaptic transistor (AiS-TSO), which was selected based on its friction capacitive coupling effect.[107] The synaptic transistor is capable of perceiving external tactile stimuli through the friction capacitive coupling effect and generating bionic neuroelectric signals by leveraging its intrinsic synaptic properties, thereby achieving the memory of external tactile stimuli. The capacitive coupling effect induced by touch stimulation alters the composition of nanocomposites within the gate dielectric layer and modulates the synaptic currents, thus enabling the memory of the intensity of external stimuli. Qing et al. report an electrochemical synaptic transistor that operates by transporting protons between a tungsten hydroxide channel and a gate, facilitated by a zirconium dioxide proton electrolyte.[104] The device can be programmed over a frequency range approaching megahertz and exhibits an endurance of over 100 million read/write cycles. Furthermore, it is compatible with CMOS technologies and can be scaled up to a lateral dimension of 150 x 150 nm^2. Through monolithic integration with silicon transistors, this work demonstrates the feasibility of creating pseudo-crossover switch arrays for energy-efficient deep learning accelerator applications.

The development of neuromorphic devices begins with initial stages involving mathematical and computational modeling, gradually transitioning to the realization of complex functionalities, thereby laying a solid theoretical foundation for subsequent practical exploration. On this basis, neuromorphic devices implement the simulation of biological synaptic plasticity, marking an important step towards intelligent simulation. As a crucial juncture in biological neural networks, the dynamic adjustment capability of synapses is vital for the transmission and processing of information. Researchers subsequently focused on optimizing the device's structure and exploring physical mechanisms to enhance its endurance

and performance. Through a combination of carefully designed structures and materials, the endurance and stability of the devices were significantly enhanced, while energy consumption was reduced.[98,108] Additionally, with the application of advanced nanotechnology and 2D materials, the integration and flexibility of the device have been significantly improved, making the neuromorphic system more compact, flexible, and adaptable to a wide variety of application scenarios. In recent years, the development of neuromorphic devices has taken a qualitative leap, achieving a breakthrough in multimodal sensing and CMOS compatibility. Multimodal sensing technology allows devices to simultaneously capture and process information from various senses, such as vision, hearing, and touch, significantly enhancing the system's perceptual ability and intelligence.[109,110] On the other hand, CMOS compatibility enables neuromorphic devices to integrate seamlessly with existing semiconductor processes. These technological advancements have laid a solid foundation for the application of neuromorphic devices in biomedical engineering.

4. Neuromorphic device based biomedical engineering technology

Currently, the application of neuromorphic devices in biomedical engineering mainly focuses on four areas: biomedical sensing technology, medical imaging diagnosis, rehabilitation medical engineering, and neural and brain-computer interface technology, as shown in Fig. 3. The following introduces neuromorphic devices within the context of these four biomedical engineering domains.

4.1. Biomedical sensing technology

Biomedical sensing technology employs aptamers specific to biomolecules (e.g., proteins, nucleic acids) as sensitive interfaces to achieve signal conversion and detection analysis through interaction with target molecules.[111,112] This detection technology typically comprises three components: a sensitive signal detection interface, a biosensor, and a signal processing system. The sensitive signal detection interface is responsible for initiating specific reactions with the analyte, while the biosensor translates these biochemical reactions into detectable electrical signals. The signal processing system then handles amplification and analog-to-digital signal conversion. Biomedical sensing technology demonstrates extensive application prospects across various fields, including medical diagnosis, environmental monitoring, food safety, and industrial process control. In medical diagnosis, it is primarily utilized for point-of-care testing (POCT), early disease detection, and home monitoring. Instant diagnostic devices, such as blood glucose meters, cardiac marker detectors, and rapid detection tools for the novel coronavirus, along with implantable or wearable biosensors, are capable of monitoring changes in physiological parameters and disease indicators of patients, thereby providing doctors with a timely diagnostic foundation. The low-power consumption characteristics of neuromorphic devices render them promising for a diverse range of applications in biosensing technology, particularly in scenarios that demand prolonged monitoring and the use of portable devices.[113,114] In wearable biosensors, low-power neuromorphic devices can extend the device's endurance and enhance

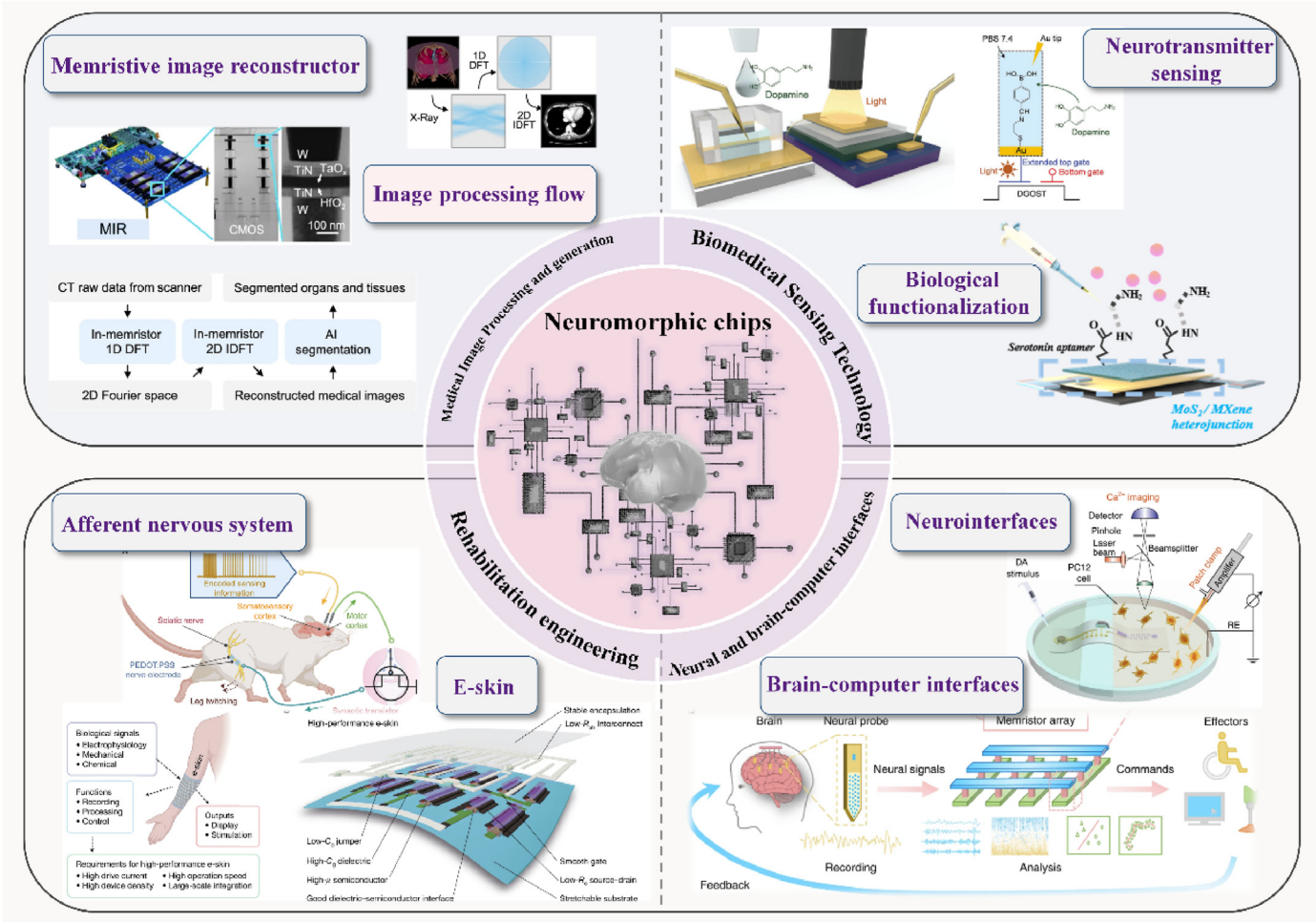

Fig. 3. Applications of neuromorphic devices in biomedical engineering. Divided into four areas: biomedical sensing technology, medical image diagnostics, rehabilitation medical engineering, and brain-machine interface technology. Copyright 2021, Wiley-VCH GmbH.[105] Copyright 2024, Springer Nature.[115] Copyright 2022, Springer Nature.[116].

user comfort and convenience. Furthermore, by leveraging the highly sensitive characteristics of carrier transport, these devices can more accurately detect and respond to weak biological signals, thereby enabling precise monitoring and analysis of subtle physiological signals in living organisms.

Oh et al. developed a dual-gate organic synaptic transistor platform, which incorporates a photoconductive polymer semiconductor, a ferroelectric insulator of P(VDF-TrFE), and an extended-gate electrode functionalized with boronic acid. This platform is designed for simultaneously detecting neurotransmitters (dopamine) and light, as illustrated in Fig. 4(a).[105] Fig. 4(b) depicts the experimental steps necessary to form a boronic acid self-assembled monolayer (SAM) on the extended gate electrode. DREGE functionalized with BA terminal groups was able to detect dopamine via the esterification process between diols and dopamine on the BA groups. Fig. 4(c) and (e) display the results of operating the bottom gate electrode ($V_{pre} = -1$ V) and top gate electrode ($V_{BGS} =$

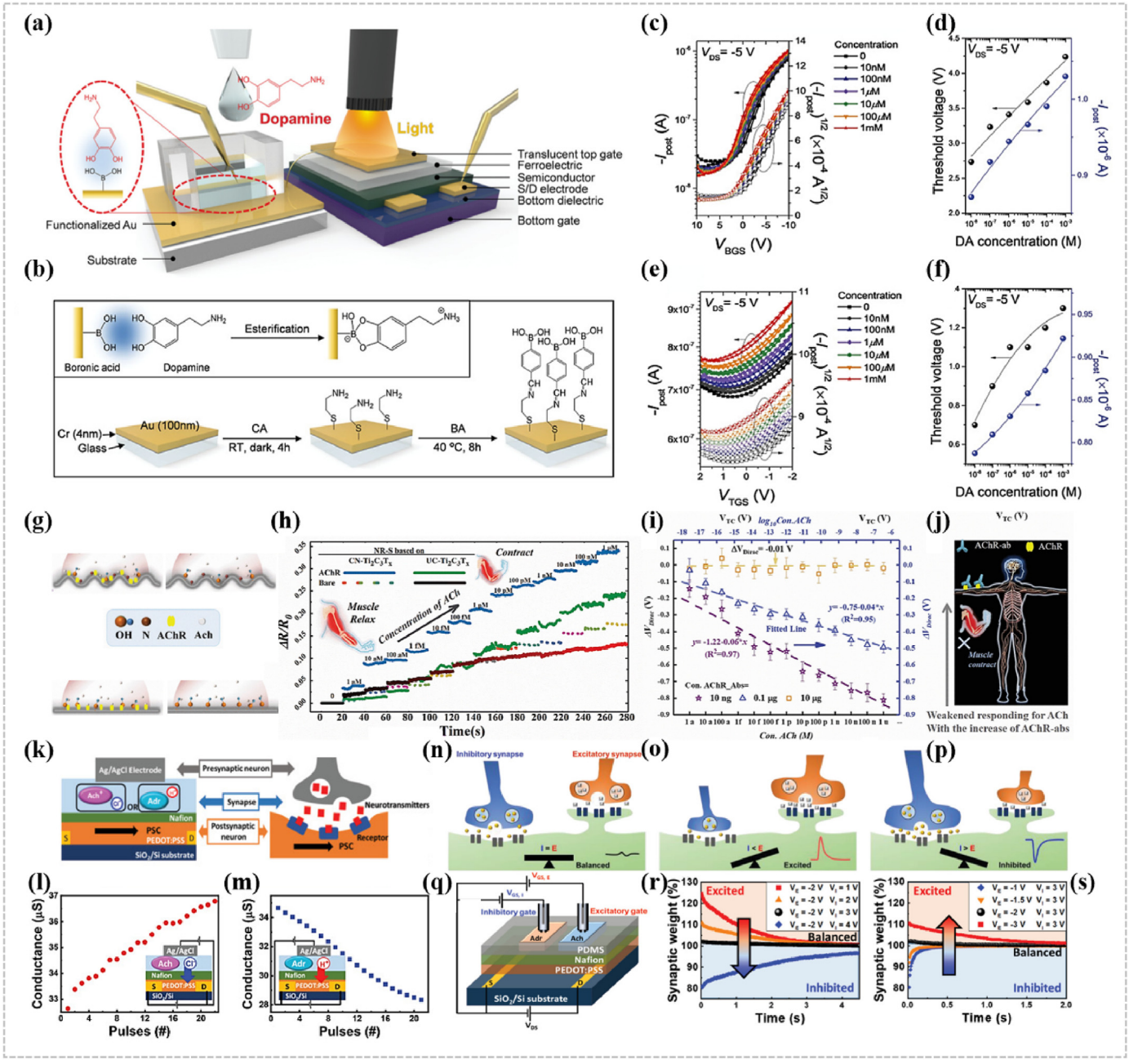

Fig. 4. (a) dual-gate organic synaptic transistors with dopamine-responsive extended-gate electrodes that can be modulated by both dopamine and light. (b) Schematic illustration of the surface functionalization step achieved by exposing Au thin film to CA and BA solutions in sequence. The upper-left panel presents a dopamine-detection process. (c)–(f) Bottom-gate (c, d) and top-gate (e, f) transfer curves and the summarized factors of the electrical changes with respect to dopamine concentrations in PBS of $10 \times 10^{-9} - 1 \times 10^{-3}$ M. Copyright 2021, Wiley-VCH GmbH.[105] (g) The illustrations for the captured ACh molecules on the different kinds of solution-MXene interfaces. (h) The linearly fitted curves of $\Delta R/R_0$ versus Con. ACh for the AChR modified devices, in contrast to the scattered data of the bare ones. (i) The shifted voltages of Dirac points (ΔV_{Dirac}) versus Con. ACh curves. (j) The schematic diagram for the damaged neuron. More AChR are injured by AChR-ab, more neuronal severity is produced, then the normal responding (muscle contract, as an example) to the increased ACh will be inhibited. Copyright 2021, Wiley-VCH GmbH.[94] (k) Schematic illustrations of the structures of the artificial and biological synapses. The gate electrode functions as the presynaptic neuron, the solution functions as the synapse, and PEDOT:PSS channel functions as the postsynaptic neuron. (l) Excitatory responses of the device with the acetylcholine. (m) Inhibitory responses of the device with the adrenaline solution. Copyright 2022, Wiley-VCH GmbH.[118].

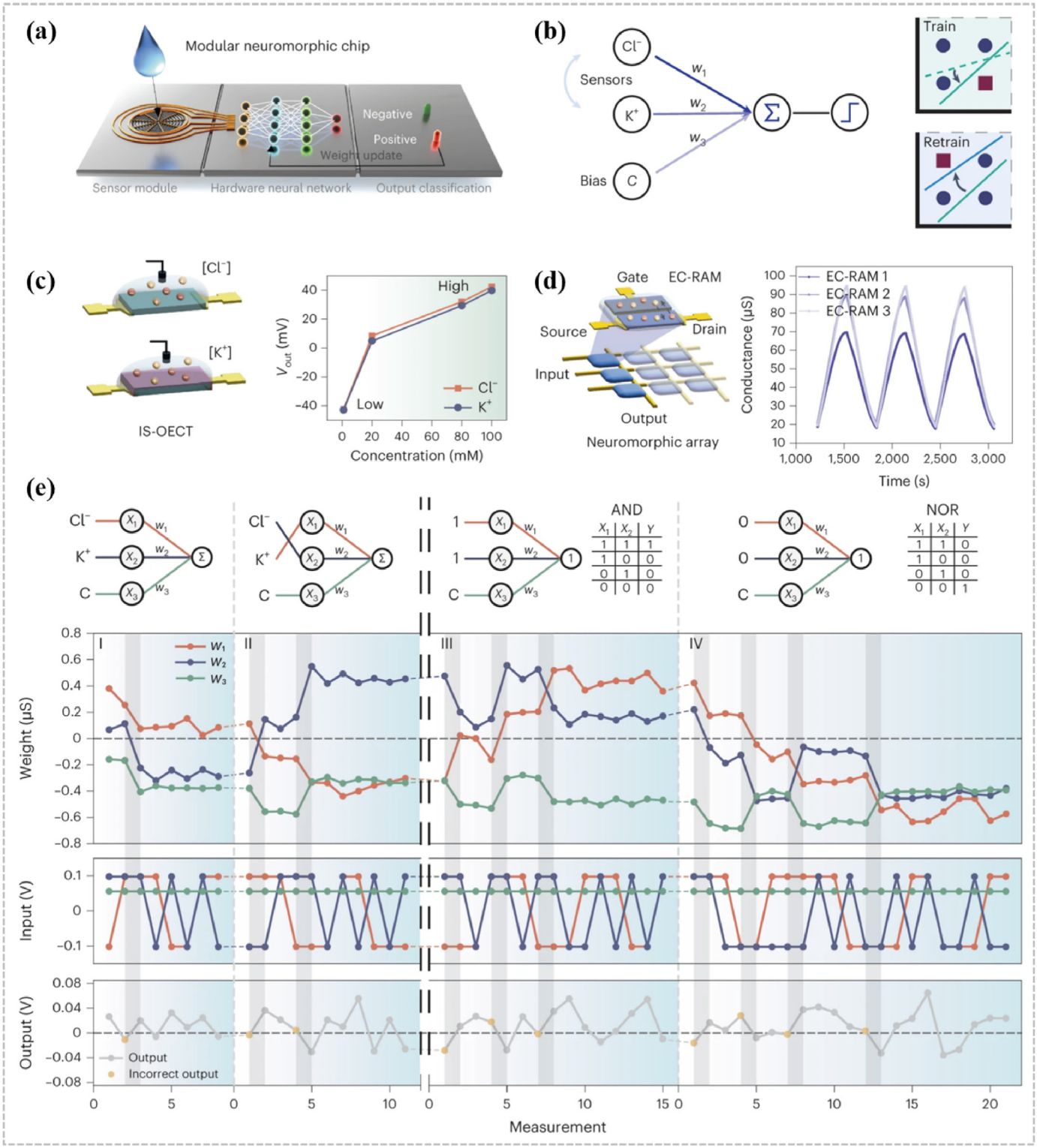

Fig. 5. (a) Illustration of the modular biosensor with distinct functions. (b) Single-layer neural network (perceptron) with sensor inputs and linear classification for trained and retrained input values. (c) Depiction of the IS-OECT sensors manipulated with and without an ion-selective membrane for measuring the K and Cl^{+-} concentrations. Sensor output versus ion concentration after the current-to-voltage module. (d) EC-RAM as part of a small neuromorphic array and the conductance values for the three EC-RAM devices used as synaptic weights. Copyright 2023, Springer Nature.[119].

−1 V) when exposed to varying dopamine concentrations in PBS. In the presence of increasing dopamine concentrations, the postsynaptic current (I_{post}) and threshold voltage increased slightly at both the bottom and top gate biases, as illustrated in Fig. 4(d) and (f) This suggests that potentiometric detection of dopamine results in a change in the charge density on the extended top gate electrode. Consequently, specific binding based on esterification is achieved at this electrode, enabling the specific recognition of dopamine. A novel three-terminal artificial synaptic device (NR-S), mediated by neurotransmitter receptors, was proposed by Wang et al.[94] By modifying the acetylcholine receptor (AChR)

at the solid-liquid interface of the newly constructed third terminal MXene-PBS, a biologically inspired simulation of synaptic plasticity behavior was achieved. As shown in Fig. 4(g), the electrical and sensing properties of the device were significantly enhanced by crumpled MXene nanosheets. Inspired by the biological synaptic signaling mode, AChR was used for testing the sensing property of the NR-S device by modifying it at the third-terminal MXene-PBS electrode interface, as illustrated in Fig. 4(h). It was found that NR-S devices based on crumpled MXene nanosheets could produce resistivity changes at ultra-low acetylcholine (ACh) concentrations (1 aM) after AChR modification, which was 10^3 times lower than that of NR-S devices based on flat MXene nanosheets. With increasing ACh levels (from 1 aM to 1 μM), the device conductivity shows an increasing trend. This sensing property of NR-S-based devices is similar to the plastic behavior of neural synapses. When continuing to modify the damaging autoreceptor antibody (AChR-ab), as the amount of antibody increased, the sensing range of the NR-S device for neurotransmitters decreased, and the sensitivity for neurotransmitter detection also decreased, as shown in Fig. 4(i). This result is similar to the neuronal damage behavior observed in neuromuscular transmission disorders (Fig. 4(j)), and provides a viable strategy for future detection of myasthenia gravis.[117] Overall, this work provides an important reference for the diversification of neuromorphic chips.

Lee et al. reported a synaptic transistor that contains an aqueous solution of neurotransmitter, Nafion, PEDOT:PSS, and electrodes, as shown in Fig. 4(k).[118] Two neurotransmitters, acetylcholine and epinephrine, were subsequently used to model the excitatory and inhibitory features, respectively. As shown in Fig. 4(l), when a positive gate voltage is applied, cations from the epinephrine solution intercalate into the PEDOT:PSS channel. Due to the presence of these intercalated ions, the distance between the PEDOT:PSS backbones increases, leading to a decrease in conductance. Therefore, an excitatory response is observed when exposed to acetylcholine solution. On the other hand, the device exhibited an inhibitory response to epinephrine solution. Inhibitory synapses were simulated when a positive voltage pulse (ranging from 6 to 9 V, with a step size of 150 mV and a pulse width of 0.1 s) was applied to the gate electrode, as shown in Fig. 4(m). As depicted in Fig. 4(n), when excitatory and inhibitory presynaptic inputs are balanced, the postsynaptic neuron's response remains within the saturated range. In this saturated state, the synaptic inputs applied to the postsynaptic neuron, both excitatory and inhibitory, are of comparable strength. These excitatory and inhibitory responses counteract each other, establishing a state of equilibrium. When the amplitude of the excitatory stimulus increases, the postsynaptic neuron transmits an excitatory signal, as illustrated in Fig. 4(o). Meanwhile, when the inhibitory stimulus is stronger than the excitatory stimulus, the postsynaptic neuron transmits an inhibitory signal, as illustrated in Fig. 4(p). To simulate these excitatory-inhibitory equilibrium properties, acetylcholine and epinephrine solutions were used to represent excitatory and inhibitory presynaptic neurons, respectively, which were then dropped into the PEDOT:PSS channel. Positive and negative voltage pulses were applied to the solutions containing acetylcholine and epinephrine, respectively, to obtain the equilibrium properties, as shown in Fig. 4(q). The inhibitory dominance operation was simulated by applying an excitatory input at an amplitude of -2V, while gradually increasing the amplitude of the inhibitory pulse from 1V to 4V (Fig. 4(r)). As the strength of the inhibitory presynaptic input increased, the device transitioned from transmitting an excitatory to an inhibitory signal. These equilibrium properties can also be modeled under conditions where excitatory inputs dominate, as illustrated in Fig. 4(s). This makes neuromorphic devices promising candidates for building complex computational systems with balanced excitatory and inhibitory functions.

In the biomedical field, post-analysis, in addition to single-target and dual-target molecular detection, can offer robust support for early diagnosis of diseases, prognostic evaluations, and monitoring of drug efficacy.[120] A neuromorphic biosensing platform capable of on-chip learning and classification is reported by Burgt et al.[119] The modular biosensor consists of a sensor input layer, an integrated array of organic neuromorphic devices that form the synaptic weights of a hardware neural network, and an output classification layer, as shown in Fig. 5(a). Fig. 5(b) shows a single-layer neural network with sensor inputs and linear classification of the input values used for training and retraining. The classification is based on a perceptron algorithm for supervised learning of binary data and defines a set of 'high' and 'low' concentrations of chlorine and potassium to represent the labeled sweat samples (Fig. 5(c)). Commercially available ion-selective electrodes and ion-selective organic electrochemical transistors (OECTs) were used to detect physiological levels of potassium and chloride, and served as input signals to the neural network on the biosensor chip, as shown in Fig. 5(d). The OECTs are in contact with an electrolyte immersed in the gate electrode, and through the gate potential, ions can be injected into the channel to change the doping state of the film, thereby altering the conductivity of the device. To further demonstrate the versatility of hardware neural network circuits and their potential as modular neuromorphic biosensors, a fully trained system was retrained on-chip after reorganizing the various inputs, as shown in Fig. 5(e).

To reduce the number of updates needed for the training process, the input signals were scaled such that 0.1 V represented a high input and −0.1 V represented a low output. In the first training cycle (Cycle I), the chloride sensor and potassium sensor served as inputs X1 and X2, respectively. Once the neuromorphic circuit was fully trained to correctly classify cystic fibrosis, the neuromorphic device exhibited electrical conductance such that the weights accurately separated the different cases. Immediately thereafter, in the second training cycle (Cycle II), the sensors were connected to different inputs of the neuromorphic circuit, with the potassium sensor serving as input X1 and the chloride sensor serving as input X2. However, in this scenario, the system once again produced incorrect outputs. The weights are readjusted to further train the circuit until the disease can be correctly classified once again, ensuring that all input samples produce accurate outputs. This demonstrates the versatility of on-chip learning, which can utilize any type of sensor in combination with labeled data. Furthermore, this approach can be extended to classify signals even when data separation is not readily apparent. Similarly, the same neuromorphic circuit can be configured to form arbitrary logic gates (e.g., AND and NOR) based on their respective truth tables. In Fig. 5(e), the author continue to sequentially train the programming of multiple logical operators. This means that they are first programmed to exhibit AND-gate behaviors (as shown in Fig. 5(e), cycle III) and are subsequently reprogrammed to exhibit NAND-gate behaviors (as shown in Fig. 5(e), cycle IV). Importantly, all training cycles were conducted without the use of a computer or software program, entirely on-chip, thereby highlighting the versatility of locally programmable neuromorphic devices for both classification tasks and dynamic logic circuits. This work underscores the versatility of low-power and easily tunable organic neuromorphic devices in real hardware arrays and circuits, which can be utilized to develop adaptive biosensors and optimizable edge computing devices. However, current neuromorphic devices still face considerable challenges in signal processing, including the need for higher temporal resolution and adaptive noise rejection. Furthermore, while these devices can compensate for shortcomings through event-driven processing and parallel computing, they still need to address the bottleneck of optimizing on-chip integration for interfacing with traditional biosensors.

4.2. *Medical image processing and generation*

4.2.1. *Medical image processing*

Diagnostic medical imaging is a widely utilized technology in the medical field today. It employs advanced imaging techniques and equipment, such as X-rays, CT, MRIs, and positron emission tomography (PET), to generate detailed images of the body's internal structures and tissues.[121,122] By analyzing these images, doctors can accurately diagnose diseases, assess the severity of conditions, and plan effective treatment

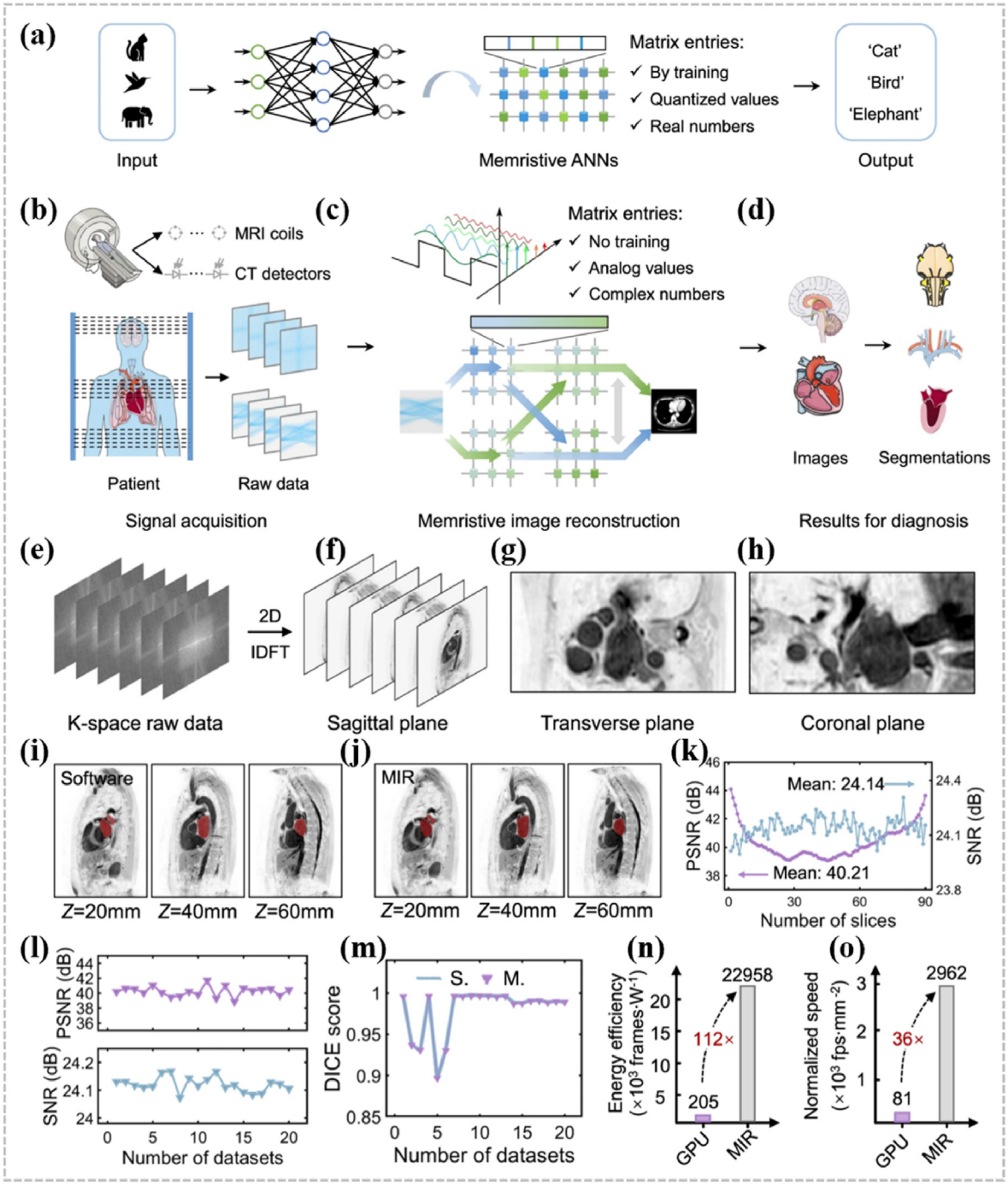

Fig. 6. (a) Memristive ANNs. The matrix entries of ANNs are obtained by training and they are usually quantized before being mapped to memristor arrays, resulting in quantization errors. Besides, most ANNs are computed in real number fashion. (b)–(d) Memristive medical imaging system. (b) Medical signal acquisition. Explosive amount of raw data is acquired from medical scanners such as magnetic resonance imaging (MRI) and computed tomography (CT). (c) Memristive image reconstruction. The matrix entries used in signal processing algorithms here are pre-calculated without training, making them more susceptible to the non-ideal device characteristics of memristors. In addition, their entries are usually expressed in analogue manner with both real and imaginary parts, requiring a completing different mapping strategy onto memristor arrays. (d) Results for medical diagnosis. Medical images of human body are reconstructed from raw data and then further segmentation and diagnosis can be performed. The cartoon pictures of human organs and medical equipment used in b and d was partly generated using Servier Medical Art, provided by Servier, licensed under a Creative Commons Attribution 3.0 unported license.

options. For instance, using equipment like X-rays, CT, and MRIs, doctors can non-invasively examine patients and obtain pertinent information on issues such as organ function, tumors, infectious diseases, and bone fractures. Neuromorphic devices have demonstrated numerous advantages in medical image diagnostics, not only in terms of high speed and accuracy, but also in their exceptional ability to process complex image data and significant improvements in energy efficiency. Compared with traditional computer processors, neuromorphic devices are able to identify and analyze features in images more quickly, thereby reducing diagnostic time and enhancing diagnostic efficiency. Especially when processing complex medical images, such as MRIs, neuromorphic devices are capable of identifying the area and type of lesion with greater accuracy, providing doctors with a more reliable basis for diagnosis. In recent years, memristors have been widely utilized to implement

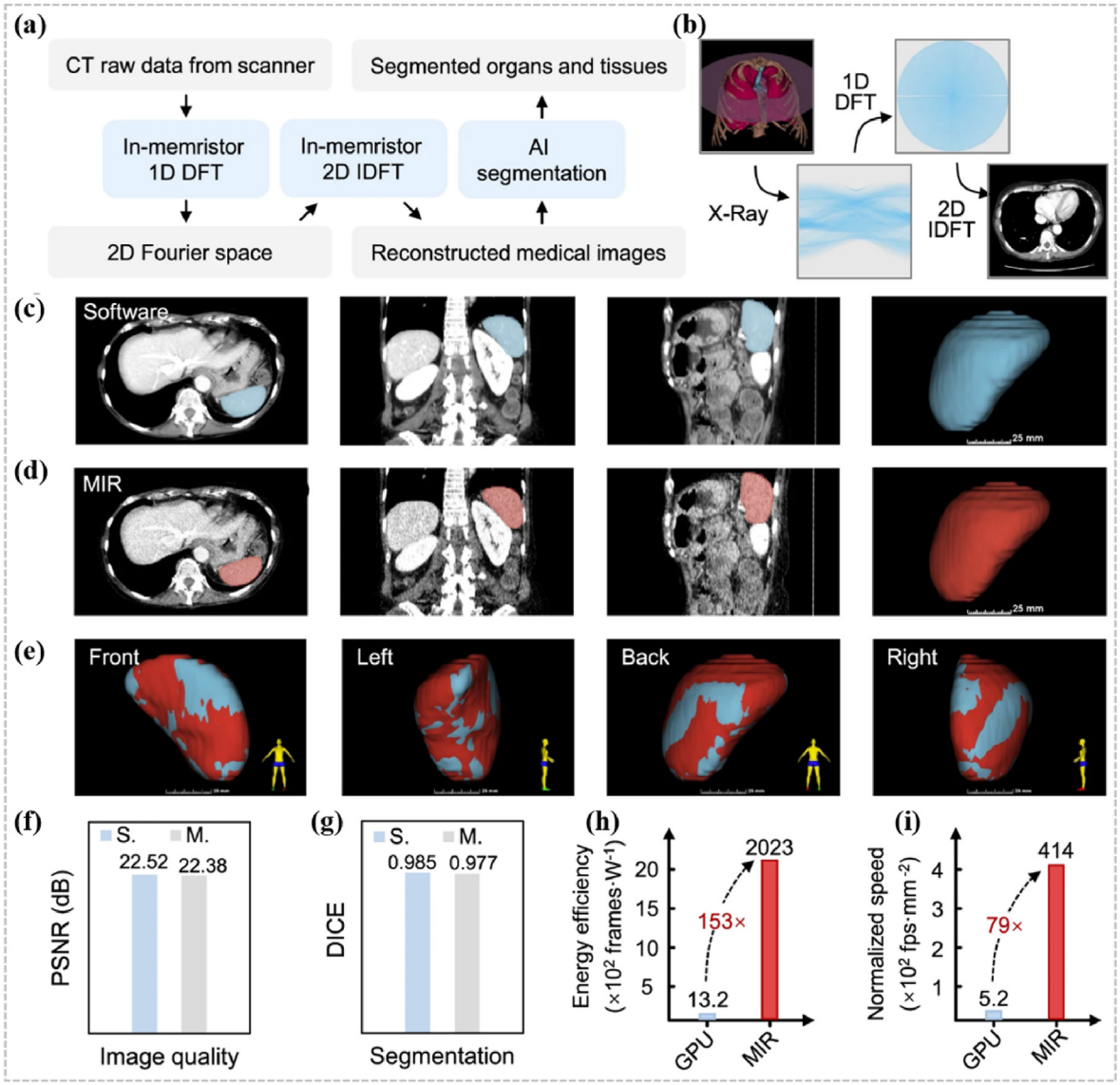

Fig. 7. (a) Schematic of CT image reconstruction with MIR followed by AI segmentation. (b) Illustration for the CT image reconstruction task. Sub-figures, from left to right, are actual human organ (the pink disc represents the section where the CT slice is acquired), projections from CT X-ray scanner, 2D Fourier space signal (intermediate results) and reconstructed CT image. (c), (d) Software-reconstructed and MIR-reconstructed 3D CT image and its segmentation results from nnU-Net (the spleen is labeled in blue and red). Sub-figures, from left to right, are sagittal plane image, transverse plane image, coronal plane image and 3D model (segmented spleen only). (e) Comparison between the segmented spleens with software-reconstructed (blue) and MIR-reconstructed (red) 3D CT images. (f) Comparison of image quality reconstructed by software (S.) and MIR (M.). (g) DICE score of nnU-Net segmented results from software-reconstructed and MIR-reconstructed images. (h) The comparison of energy efficiency of GPU and MIR. (i) The comparison of the normalized image reconstruction speed of GPU and MIR. In this context, the authors utilized the spleen dataset sourced from the Sloan-Kettering Cancer Center, which comprises 61 CT scans taken during the portal phase. Within this dataset, the spleen was initially segmented semi-automatically and then refined manually by an abdominal radiologist. Fig. 7(c) and (d) exhibit the CT images reconstructed by the software and MIR, respectively. In Fig. 7(e), the segmented 3D spleen models derived from both the software and MIR are combined and examined from four diverse angles. Only pixel-level differences can be observed on the spleen surface, indicating excellent consistency. Quantitatively, in Fig. 7(f) and (g), the PSNR values of the CT images reconstructed by the software and MIR are 22.52 dB and 22.38 dB, respectively. Similarly, the DICE scores for the segmentation results are 0.985 and 0.977, respectively. These results further confirm that MIR exhibits excellent robustness to cumulative errors and memristor device noise. Furthermore, the benchmark presented in Fig. 7(h) and **(i)** demonstrates that MIR is again 153 times more energy efficient than the GPU.

Artificial Neural Networks (ANNs), demonstrating significant advantages in terms of energy efficiency and speed compared to conventional hardware, as illustrated in Fig. 6(a).[123,124] It also has the ability to process complex MRI and CT images, as shown in Fig. 6(b). Zhao et al. proposed a memristor-based image reconstructor (MIR),[125] which accelerates the process of image reconstruction for the Discrete Fourier Transform (DFT) by utilizing an array of memristors, as depicted in Fig. 6(c). To efficiently implement the Discrete Fourier Transform (DFT) on a memristor array, the authors developed two strategies: quasi-analogue mapping (QAM) and complex matrix transfer (CMT) schemes. These schemes improve the mapping accuracy and transfer efficiency, respectively. When using QAM, the memristor-based DFT results are consistent with those obtained through software computation, in contrast to the conventional quantized mapping (QM) approach. With CMT, the memristor-based DFT requires fewer peripheral circuits compared to the traditional real-virtual separation scheme. This suggests that it holds great potential for low-power and high-speed portable medical imaging systems in future medical scenarios, as illustrated in Fig. 6(d). The authors utilized a cardiac dataset provided by King's College London,[126] which encompasses 30 three-dimensional (3D) MRI

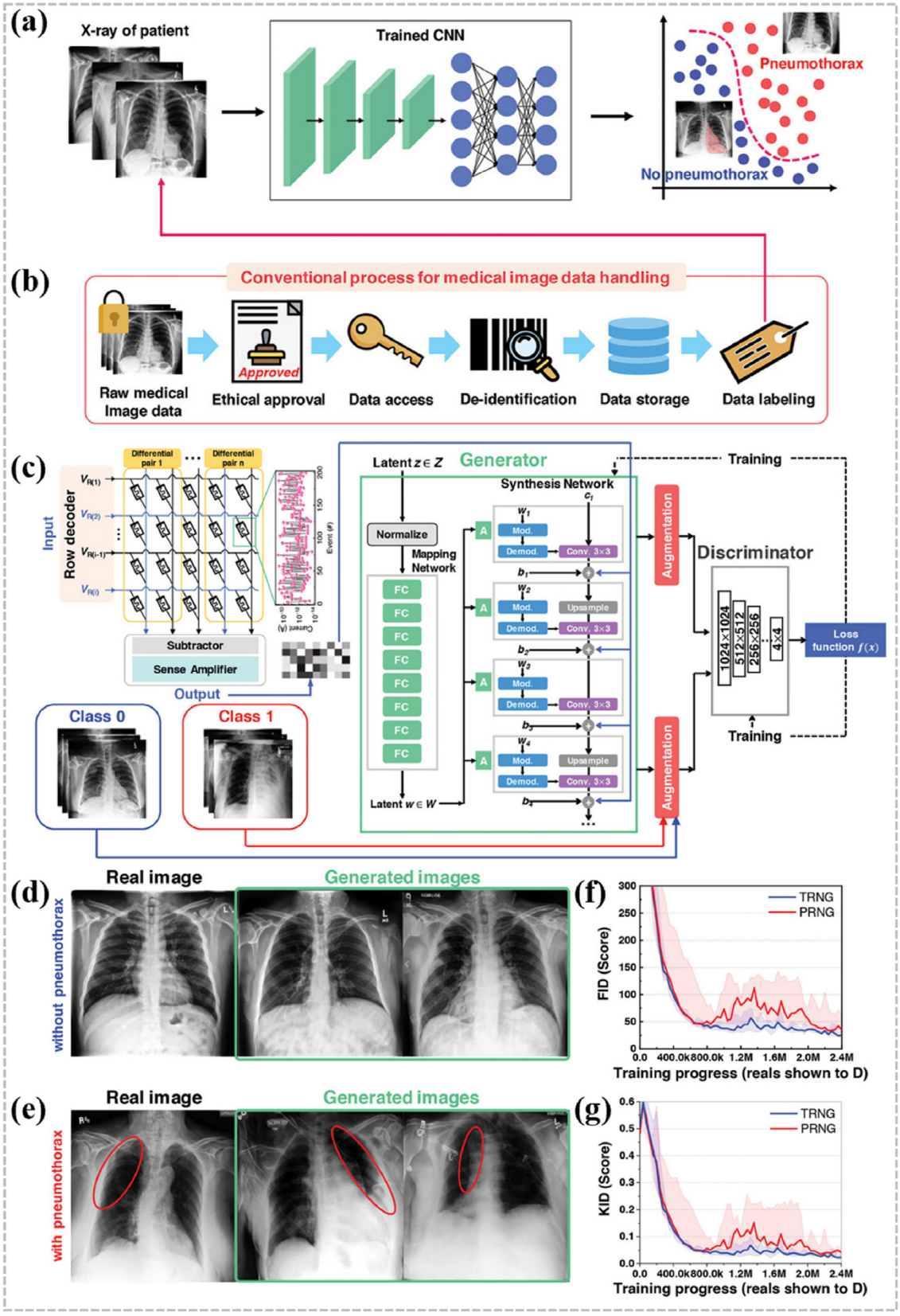

Fig. 8. (a) The framework for lesion detection using convolutional neural networks. (b) Schematic of conventional process for medical image data handling. (c) Schematic illustration of StyleGAN2-ADA using random numbers generated from mTRNG. Representative chest X-ray images (d) without and (e) with pneumothorax generated by StyleGAN2-ADA harnessing random numbers generated from mTRNG. (f) FID and (g) KID scores against the full dataset achieved by SyleGAND2-ADA using TRNG and PRNG-based random numbers during the repeated network training. The bold lines represent the median values, and the light lines show min/max scores at the each training point. Copyright 2024 Wiley-VCH GmbH.[129].

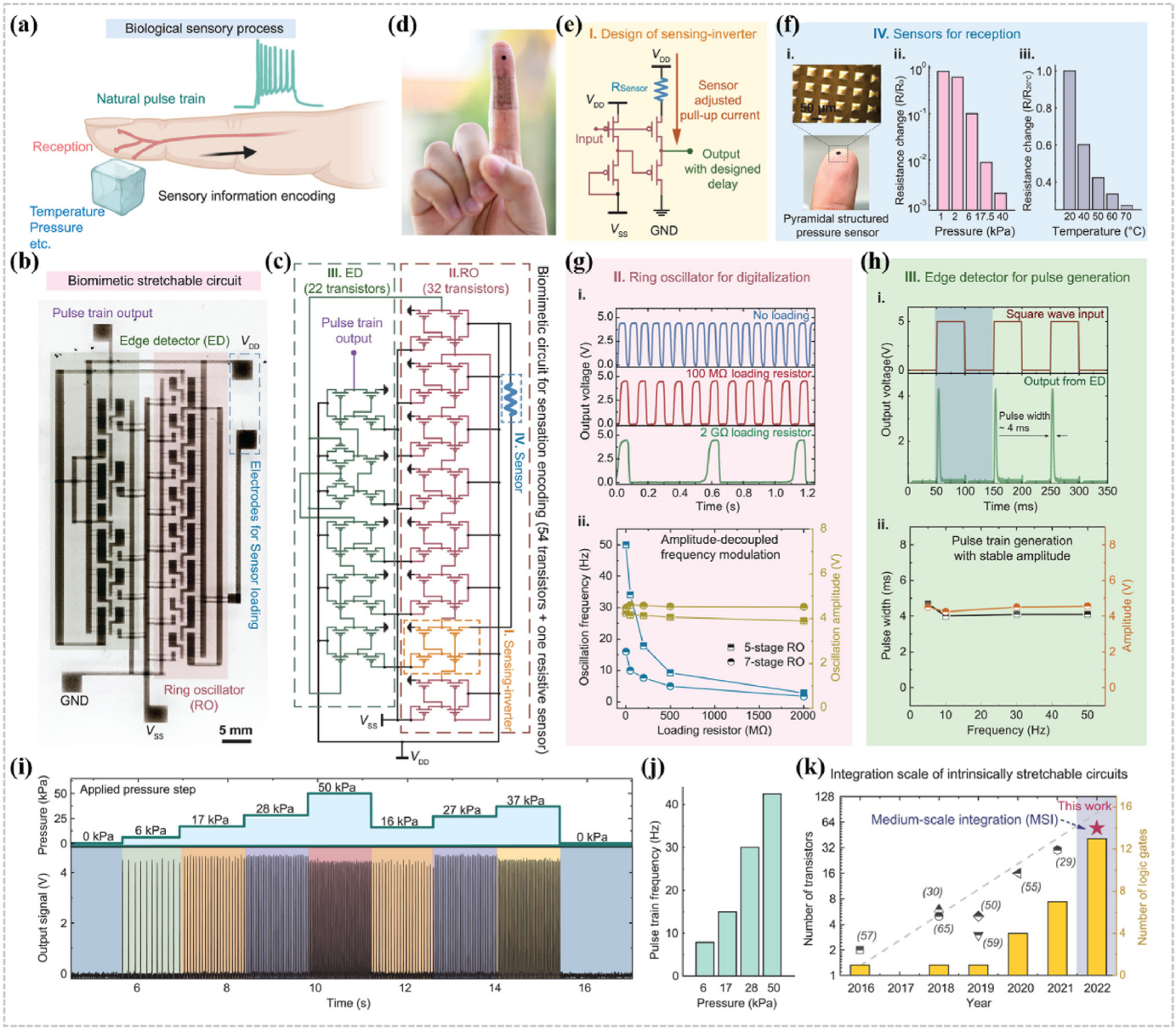

Fig. 9. Low-voltage-driven, soft circuit system for generating biomimetic pulse trains. (a) Schematic diagram showing the natural perception process. (b) Optical microscopic image of a stretchable seven-stage RO-ED circuit. GND, ground; VSS, negative power voltage. (c) Transistor circuit diagram of the biomimetic sensor-circuit system for sensory information encoding. (d) Photo of a soft e-skin attached to a finger. (e) Circuit diagram and working mechanism of the sensing inverter. (f) Panel (i) presents transfer curves showing the amplitude-decoupled frequency modulation of a seven-stage RO with different loading resistor values. The RO output frequency changed from 16 Hz at 0 Ω to 1.8 Hz at 2 gigohms. Panel (ii) shows the oscillation frequencies and amplitudes for a five- and a seven-stage RO while loading different resistors. (g) Panel (i) presents input (top) and output (bottom) signals from an ED that produces a pulse width of ~4 ms. Panel (ii) shows the averaged pulse widths (squares) and amplitudes (circles) from three different individual pulses of an ED under different input signal frequencies. Inputs are as follows: square wave, amplitude 5 V, and 50 % duty cycle. (h) Panel (i) contains a photo and magnification showing a pressure sensor with pyramidal structures. Resistance (R) changes of a pressure sensor and a temperature sensor under stimuli are shown in panels (ii) and (iii), respectively. (i) Pulse train output (bottom) from a pressure sensor–RO-ED (five-stage) system during a pressing-releasing cycle (top). (j) Output frequency of the sensor-RO-ED system under different pressures from data shown in (I). (k) Comparison of previously reported intrinsically stretchable circuits with our RO-ED circuit in terms of the integration scale level (number of transistors and logic gates). The different shapes and patterns of the symbols are used to mark the number of transistors involved in circuits from previous works, which are indicated by the reference numbers. The dashed line represents the trend of the degree of integration of stretchable electronics over time. All circuits were operated under VDD = 5 V and VSS = −5 V. Copyright 2023, The American Association for the Advancement of Science.[134].

images of the entire human heart. An expert segmented one of the left atrial images using an automated tool, followed by manual corrections. Fig. 6(e) displays the raw data sampled in K-space from the MRI scanner. A series of sagittal images were reconstructed using our memristor-based DFT (Fig. 6(f)), leading to the acquisition of the final 3D MRI images. Fig. 6(g) and (h) exhibit MRI images (cross-sectional and coronal views) observed from different angles, demonstrating good consistency across various sagittal planes. High-quality image reconstruction was then carried out by the MIR. The reconstructed MRI images and segmentation results (left atrium) are presented in Fig. 6(i) (software-based) and Fig. 6(j) (MIR-based), showing excellent agreement.

As shown in Fig. 6(h)- 6(g), the average peak SNR of MIR is 40.21 dB, while the SNR is 24.14 dB. Similar values were obtained from the other 20 MRI datasets (as shown in Fig. 6(k)), validating the high-fidelity

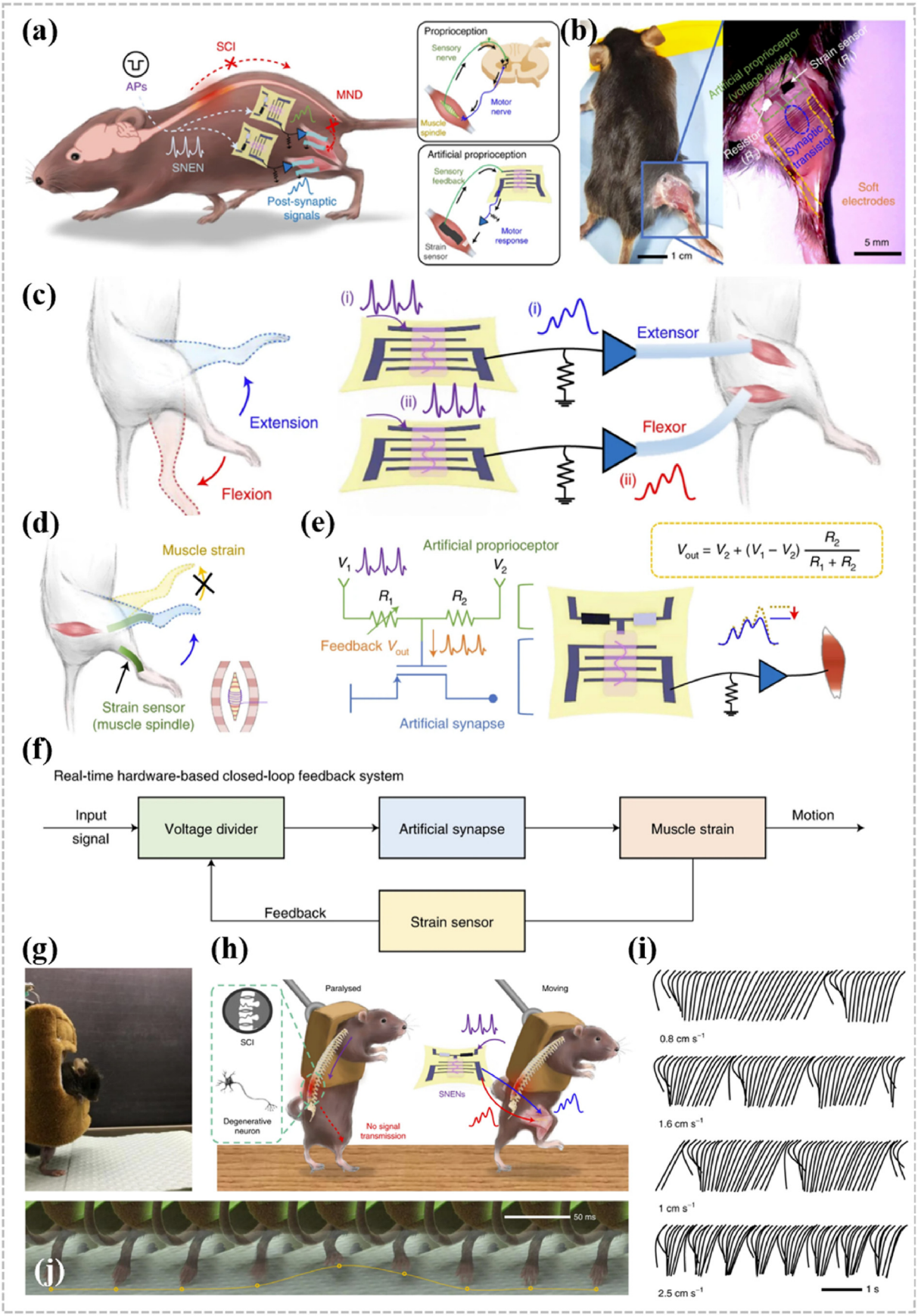

(caption on next page)

Fig. 10. (a) Schematics of SNEN based on organic electronic synapses that bypass the damaged nerves and relay neural signals to the muscle. (b) Photographs of anaesthetized mouse with SNEN attached to the leg. Flexors and extensors of the legs are electrically stimulated by post-synaptic signals through soft electrodes or needle electrodes. (c) Stimulation of an extensor and flexor of a hind leg with two artificial efferent nerves; one nerve was connected to an extensor and the other nerve was connected to a flexor. Conceptual design (d) and schematic (e) of an artificial muscle spindle-based proprioceptive feedback loop that prevents damage of muscle caused by overstraining. (f) Block diagram of the real-time hardware closed-loop feedback system of artificial proprioception. g) Photograph and (h) schematic of a paralysed mouse afflicted by SCI or MND (left) and a mouse that had recovered voluntary motor function by using SNEN (right). Practical locomotion is demonstrated with coordinated stimulation of the muscles by post-synaptic signals of the SNEN and patterned pre-synaptic AP inputs. (i) Kinematic trajectory of a hind leg with different moving speeds. (j) Photochronography of a hind leg during walking. Copyright 2022, Springer Nature.[136].

image reconstruction capability of MIR. In addition, as depicted in Fig. 6(l), the scores of images reconstructed by MIR and by software are equally high after segmentation using nnU-Net. These results suggest that MIR can exhibit excellent performance in MRI image reconstruction tasks, even in the presence of read noise and mapping errors in the memristor.

Fig. 6(m) - 6(o) further demonstrate that MIR is 112 times more energy efficient and 36 times faster in normalized image reconstruction compared to the Nvidia Tesla V100 GPU. To further check the calculation accuracy and noise robustness of MIR, author completed a more complex task: CT image reconstruction based on the Fourier center slice theorem, which involves three DFT/IDFT steps. The data processing procedure is illustrated in Fig. 7(a). During the CT scanning process, X-ray projections of a human body taken from different angles are processed to produce cross-sectional images for diagnostic and therapeutic purposes. Each projection vector is sent to MIR for DFT processing to generate a frequency domain signal in the 2D Fourier space. The reconstructed CT image can then be obtained by performing 2D IDFT on the 2D Fourier space. In the entire CT image reconstruction process, a total of three DFT steps are required to convert the original projection data into a CT image. Finally, nnU-Net can be used to segment organs or tissues from the reconstructed CT image. Finally, nnU-Net can segment organs or tissues from the reconstructed CT image. For instance, Fig. 7(b) displays the original human organs alongside the reconstructed CT images, along with intermediate results.[127]

4.2.2. *Medical image generation*

High-quality medical image data plays a crucial role in the medical field, as it can realistically reproduce medical scenarios and pathological features, providing doctors with an accurate and reliable basis for diagnosis, treatment, and surgical planning. By utilizing publicly available chest X-ray images and radiology report datasets, the model is able to generate diverse and visually plausible synthetic X-ray images. This enables visual-verbal models, which have been pre-trained on natural images, to generate diverse and realistic medical images, thereby alleviating the shortage of high-quality medical image datasets.[128]

Kim et al. reported a generative adversarial network (GAN) based on a memristor cross-switch array, which is capable of generating a large number of annotated and realistic chest X-ray images.[129] Fig. 8(a) illustrates the main framework for lesion detection utilizing a convolutional neural network (CNN), a technology that has been widely adopted for classification tasks related to medical image diagnosis.[130] The lesion detection system aids radiologists in accurately identifying diseases and facilitates automated lesion diagnosis when the patient's X-ray images are fed into a pre-trained CNN. The development of a lesion detection system using medical datasets, as well as for other research purposes, involves numerous steps, as depicted in Fig. 8(b).

To demonstrate the feasibility of generating and enhancing labeled medical images without requiring additional labeling, StyleGAN2 with adaptive discriminator augmentation (ADA) was utilized, employing random numbers generated by a memristor-based random number generator (mTRNG), as illustrated in Fig. 8(c). Fig. 8(d) and (e) display X-ray images, one with and one without pneumothorax, generated by StyleGAN2 with ADA using the random numbers supplied by the mTRNG.[131] Without using additional labeling techniques, labeled chest X-ray images were generated by simply applying the real chest X-ray images corresponding to each category to StyleGAN2 with adaptive discriminator augmentation (ADA). The StyleGAN2 ADA, trained with class 0 real chest X-ray images, generated only chest X-ray images without pneumothorax, whereas the network trained with class 1 real images generated chest X-ray images with pneumothorax. The authors then used the Fréchet Inception Distance (FID) and Kernel Inception Distance (KID) to quantitatively evaluate the performance of the network and the fidelity of the generated images. As shown in Fig. 8(f) and (g), StyleGAN2 with adaptive discriminator augmentation (ADA) using mTRNG demonstrates superior FID and KID scores compared to images generated using a pseudorandom number generator (PRNG), suggesting that mTRNG has the advantage of producing more diverse and high-quality medical images than PRNG. Furthermore, due to the highly random nature of the random numbers generated by mTRNG, the network trained with mTRNG not only converged quickly but also steadily maintained low FID and KID scores. In contrast to the network based on mTRNG, the neural network based on PRNG exhibits a relatively slower convergence speed and higher volatility, as the slight regularity in the random numbers generated by PRNG hinders the convergence results. Thus, the results indicate that mTRNG has great potential for generating privacy-sensitive real medical images and eliminates the need for labeling in the development of AI-based automated lesion diagnosis. Although neuromorphic devices show great potential in medical image processing and generation, they are still limited by the challenge of dynamically balancing device homogeneity and algorithmic accuracy. This challenge necessitates both addressing the trade-off between dynamic range compression and time-series fidelity for artificial neural networks and developing bio-inspired adaptive sampling controllers to match organ motion rhythms. In medical image generation, neuromorphic-based neural networks lack pathological knowledge, thereby generating images with spurious pathological features and compromising credibility—a gap that demands synergistic optimization across device-algorithm-system levels.

4.3. *Rehabilitation medical engineering*

As a comprehensive discipline, Rehabilitation Medical Engineering deeply integrates the essence of biomedical engineering and rehabilitation medicine, and is committed to the development of various types of rehabilitation medical equipment and appliances, such as prosthetics, orthopedic supports, functional examination and exercise equipment, etc. Its aim is to provide comprehensive rehabilitation services and support for the disabled, the injured, the sick, and other groups.[132,133] As medical demand continues to rise, the types of technologies and their implementation methods in the field of rehabilitation engineering are gradually showing a more diversified trend. This change not only reflects the continuous progress and innovation in rehabilitation engineering technology but also aligns with the contemporary medicine's requirements for individualized and efficient patient rehabilitation. Bao et al. reported a monolithic soft prosthetic e-skin that has the ability of multimodal perception, neuromorphic pulse signal generation, and closed-loop actuation.[134] In the natural perception process, somatosensory receptors convert the input stimuli into FM pulse trains with constant amplitude, ensuring efficient and high-fidelity signal transmission, as shown in Fig. 9(a). To implement this process, the authors developed a circuit system comprising a sensor for collecting external stimuli, a ring oscillator (RO) for frequency modulation of the sensor signal, and an edge detector (ED) for action potentials, as depicted in Fig. 9(b)-9(d). To

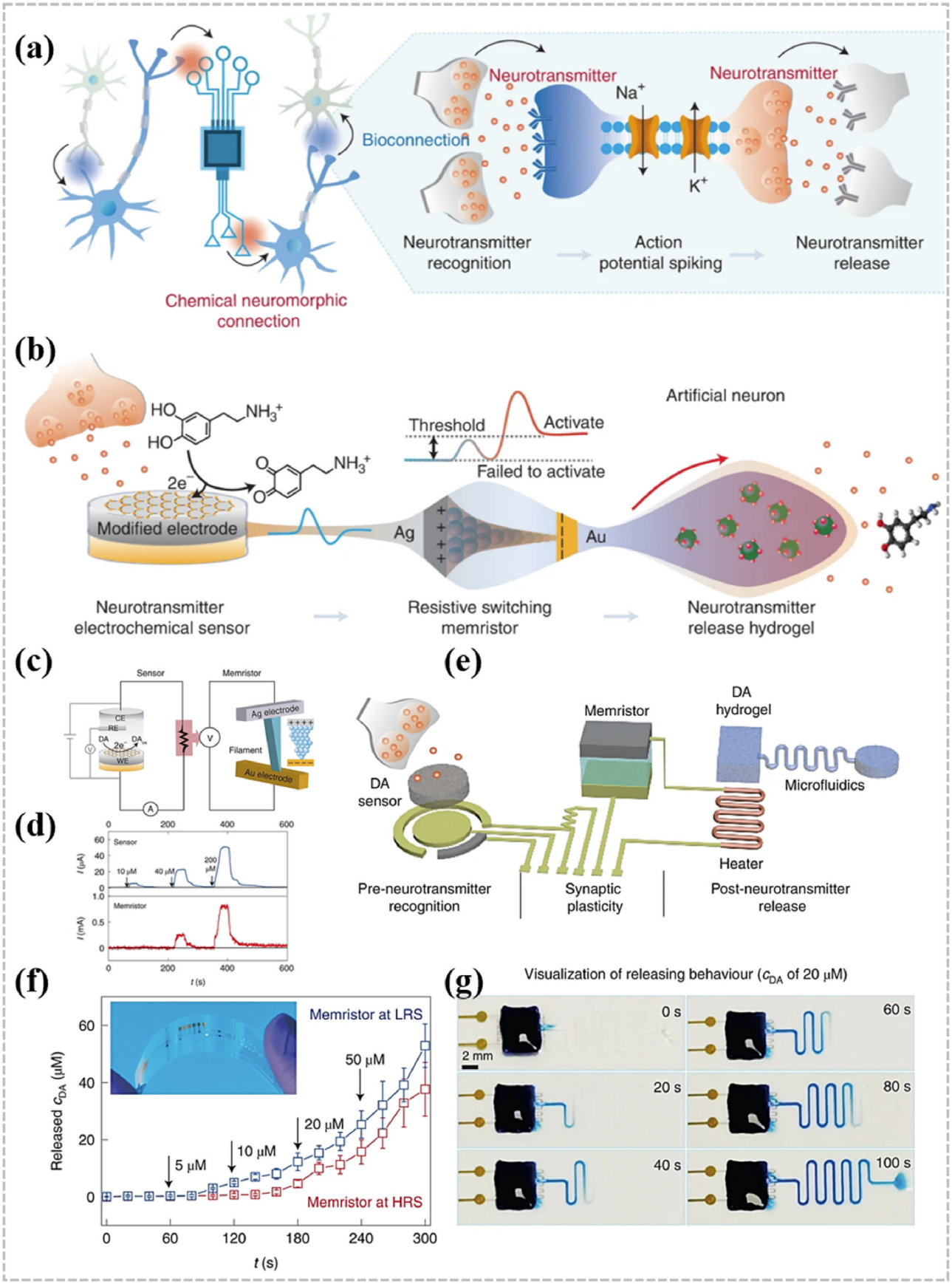

(caption on next page)

Fig. 11. (a) Schematic of a biohybrid neurointerface where artificial neurons chemically communicate with biological neurons, forming a complete neuromorphic communication loop. A biological neuron comprising neurotransmitter receptors on the dendrite to specifically recognize neurotransmitters, followed by the spiking of action potential based on ion-fluctuation-induced membrane potential changes, and the triggering of neurotransmitter release in the vesicle at the terminal of the axon. (b) An artificial neuron comprising neurotransmitter detection via an electrochemical sensor, sensory signal processing with synaptic plasticity using a resistive switching memristor device and signal-triggered neurotransmitter release based on a hydrogel component. (c) In-sensing memory based on the combination scheme of the DA sensor with the memristor. (d) Response of DA electrochemical sensor and the corresponding response of the memristor following the DA period. (e) Schematic of an artificial neuron that simulates the function of an interneuron including pre-neurotransmitter recognition, synaptic plasticity and post-neurotransmitter release. (f) Dynamic release of DA from the hydrogel induced by DA stimuli when the memristor is in the initial HRS and LRS. The inset shows the digital image of a flexible artificial neuron that contains a CNT/GO-based DA sensor, Ag NPs–silk fibroin/Au memristor, heater and PDMS-based microfluidic film. The data are presented as mean values (s.d.). The error bars are obtained from n = 3 different artificial neurons examined in independent measurements. (g) Visualization of DA-triggered releasing behaviour using methylene blue as the indicator. Copyright 2023, Springer Nature.[116].

mitigate large amplitude variations within the limited dynamic range of the frequency tuning, the sensor was positioned in the second stage of the inverter, as illustrated in Fig. 9(e). By integrating this design with the transistor's high on-off current ratio, a modulation frequency range associated with physiological signals (i.e., 0–100 Hz) was achieved, alongside a stable amplitude across a varying load resistance between 0 and 5 GΩ, as shown in Fig. 9(f). In order to better simulate the biological coding process of pulse sequences, the ED circuit was further developed to remodel the RO output signal. With a properly designed delay network and AND gate, the ED can efficiently capture the rising edge of the input signal to generate sharp pulses, as shown in Fig. 9(g)-9(i). With the optimal geometrical design of the delay network, the AND gate, and the corresponding circuits, a stretchable ED is realized that can generate stable pulse signals with a duration of 4 ms and an amplitude of 5V in response to square wave inputs of different frequencies (up to 50Hz), as depicted in Fig. 9(g). Using all the developed components, a monolithic integrated electronic skin patch as soft as human skin was fabricated to mimic natural sensory processes with driving voltages less than ±5 V, as shown in Fig. 9(b) and (c). In addition, carbon nanotube-based stretchable pressure sensors and thin-film temperature sensors with a 3D pyramidal structure were developed and integrated into the system to mimic natural mechanoreceptors and thermoreceptors, respectively, as shown in Fig. 9(h).

When applying a pressure from 0 to 50 kPa or changing the temperature from 22 °C to 90 °C, burst signals are generated and emitted faster depending on the pressure and temperature stimulus levels, as shown in Fig. 9(i) and (j). The above e-skin circuit, consisting of 54 stretchable transistors, achieves medium-scale integration of stretchable organic electronics, as shown in Fig. 9(c) and (k). A biological sensorimotor circuit was simulated using the e-skin. When a progressively increasing pressure stimulus is applied, the solid-state synaptic transistors generate a stronger driving current, while the induced motor signals simultaneously stimulate the sciatic nerve. Through the artificial synapses, these signals will activate the downstream muscles, completing the artificial sensorimotor loop. This loop shows significant potential for next-generation robots and medical devices.

In order to achieve complex movements, organisms have evolved complex nervous systems. Damaged nervous systems can lead to poor transmission of biological signals, resulting in the loss of some or all bodily functions.[135] Repairing the damaged nervous system in humans has long been a challenge in medicine and the biological sciences. However, conventional functional electrical stimulation (FES) has limitations and often requires complex digital circuits and computers to control the stimulation model and stimulate gentle muscle movements. It also requires the patient to carry the appropriate equipment during the computation process and is not suitable for long-term use by patients in their daily life. Lee et al. designed a stretchable, low-power artificial neural synaptic device with feedback function by modelling the neural feedback structure of biologically controlled muscle movements.[136] The concept of the stretchable neuromorphic efferent nerve (SNEN) is to avoid the damaged nerve and send neuromorphic electrical signals to the muscle, thus replacing the damaged nerve, as shown in Fig. 10(a). The SNEN consists of stretchable components, including carbon nanotube (CNT) strain sensors, organic semiconductor nanowires, and ion-gel stretchable synaptic transistors, as well as soft hydrogel electrodes. To demonstrate the concept, the SNEN was attached to the legs or backs of mice, as shown in Fig. 10(b). To simulate synchronous movements, two synaptic transistors were connected to the flexor and extensor muscles, respectively, as shown in Fig. 10(c). Alternating input action potentials with a frequency of 50 Hz (f_{AP} = 50 Hz) were applied to the synaptic transistors at 1-s intervals. Each muscle was stimulated to stretch and flex alternately, enabling leg displacement. Subsequently, an artificial homeoreceptor was demonstrated for detecting leg movements and preventing muscle overstretching, as shown in Fig. 10(d) and (e). The artificial homeoreceptor, in conjunction with the artificial synapses, formed a closed-loop feedback system, as depicted in Fig. 10(f). The feasibility of using SNEN in actual exercise was subsequently tested, as demonstrated by a mouse suspended by a vertical brace, as shown in Fig. 10(g). The input signal was applied to the synaptic transistor of the right hind leg extensor muscle, and this signal was modulated to control the leg swing and induce a sharp contraction of the extensor muscle through the EPSC. A bipedal walking motion was also achieved, as shown in Fig. 10(h). After connecting one synaptic transistor to the flexor muscle of the left leg and the other to the extensor muscle of the right leg, and similarly connecting the second transistor to the extensor muscle of the left foot and the flexor muscle of the right foot, bipedal walking movement was induced by alternating input signals from each SNEN.

By adjusting the input action potentials (APs), the movement ranged from slow walking to running on a treadmill, as shown in Fig. 10(i) and (j). The power required for this artificial synaptic control of muscle movement is just 1/150 of that required by the functional electrical stimulation method. By utilizing stretchable artificial nerves, the motor function of the legs of a mouse suffering from a neuromotor disorder can be restored, enabling it to kick a ball, walk, or run. This represents a significant breakthrough in overcoming nerve damage and opens up new avenues for enhancing the quality of life for patients with related diseases. The technological evolution of rehabilitation medical engineering has posed multidimensional challenges to neuromorphic devices: at the hardware level, this requires both the construction of millisecond-level motion-sensing closed-loop systems for precise bionic control of prostheses and breakthroughs in maintaining synaptic plasticity under sustained mechanical loading. Meanwhile, the fundamental conflict between biocompatibility and high-density sensing integration continues to hinder the clinical translation of haptic interfaces. In the algorithmic dimension, the imbalance between nociceptive inhibition and proprioceptive enhancement in neurofeedback systems risks misaligning motion perception during prolonged use, while bottlenecks in cooperative learning between EMG signals and neuromorphic networks have stalled the dynamic adaptation of rehabilitation devices. This multilevel technical challenge not only catalyzes cross-disciplinary integration among materials science, biomechanics, and neuroengineering but also drives the development of innovative paradigms such as bionic tactile interfaces and adaptive closed-loop regulation in rehabilitation medicine.

4.4. Brain-machine interfaces

Brain-machine interface (BMI) captures brain signals and converts them into electrical signals, thereby realizing visual detection of these

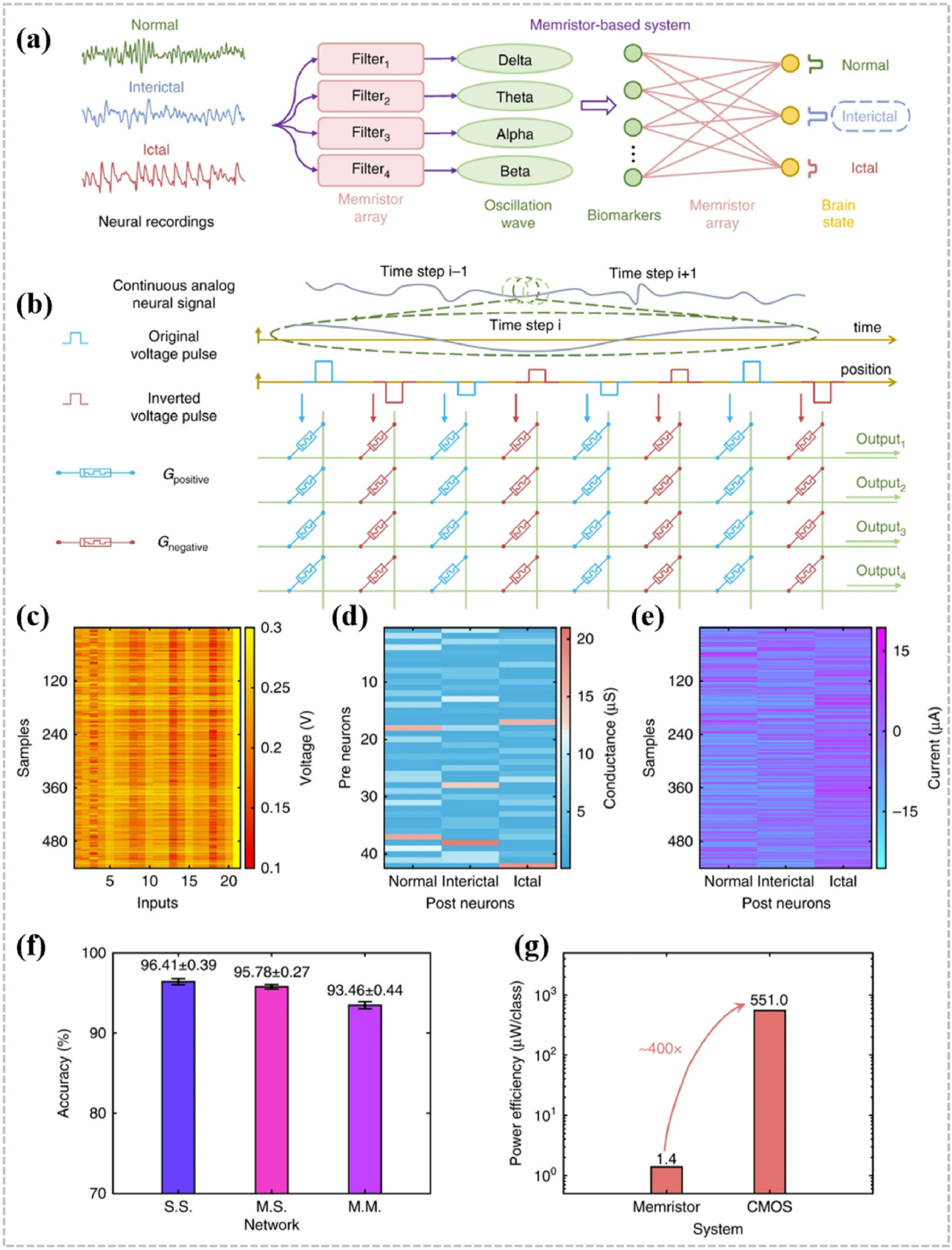

(caption on next page)

Fig. 12. (a) Schematic of the memristor-based system to identify epilepsy-related brain state. Normal, interictal, and ictal neural activities are filtered by the memristor array to obtain oscillation waves in δ, θ, α, and β frequency bands. Biomarkers extracted from the filtered waves are used to identify the brain state through a single-layer neural network, which is implemented in another memristor array. (b) Implementation of the filter bank for neural activities in a memristor array. Continuous analog neural signal is conditioned and sampled as voltage pulses, which are applied to the input columns of the memristor array. Here Gpositive and Gnegative represent the memristor conductance for positive and negative weights, respectively. (c) Input voltages transformed from the extracted biomarker vectors to be applied on the memristor array-implemented neural network. (d) Conductance map of the memristor array for the single-layer perceptron neural network. (e) Output current of the neural network. The output neuron with the largest current value shows the input signal type. (f) Overall accuracies of the software-simulated and memristor array-implemented neural networks in the identification of the brain state. Here, error bars represent the standard deviations. S.S. represents the network trained using software-calculated results. For M.S. and M.M., the networks are trained using memristor array-filtered results, and M.S. uses the software-simulated network while M.M. uses the memristor-implemented network for inference. (g) Comparison of the power efficiency for CMOS-based and memristor-based systems.

brain signals.[137] BMI can be categorized into two types: implantable BMI and non-implantable BMI. For implantable BMI, the signal acquisition device (electrode) is directly implanted into the patient's cerebral cortex through surgery or other means. This method boasts high accuracy, high temporal resolution, and a high information transmission rate, among other advantages. However, it also poses challenges such as high surgical risk, a high infection rate, and significant implantation trauma. Non-implantable BMI does not require surgery and can collect brain signals directly from outside the brain. However, at the same time, due to the signal attenuation caused by the skull and the blurring effect of electric field dispersion, the signal resolution is low, making it difficult to identify the brain area or individual neurons associated with the signal emission. Additionally, the signal cannot be transmitted if the conductive paste fails.[138] Therefore, the development of new BMIs becomes particularly important for the transmission of neural signals. Chen et al. reported on a chemically mediated artificial neuron that can receive and release the neurotransmitter dopamine.[116] As shown in Fig. 11(a), neurons in the human brain communicate with each other through synapses, and neurotransmitter-mediated synaptic plasticity behaviors occurring in the synaptic gap induce emotional and memory behaviors.[139,140] To enable chemical communication between biological neurons, bioelectronics must possess at least three fundamental functions: neurotransmitter identification, synaptic plasticity simulation, action potential excitation, and neurotransmitter release. For the implementation of such chemically mediated artificial neurons, three modules, a DA electrochemical sensor, a resistive switching memristor, and a thermally induced DA release hydrogel, were constructed, as illustrated in Fig. 11(b). Electrochemical sensors convert chemical signals into electrical signals and affect the memristor. The resistive state of the memristor is modulated by DA as a signal, which can mimic the STP and LTP of synapses. A polymer hydrogel with temperature-dependent properties was used to simulate how interneurons release DA. In this artificial neuron, the DA electrochemical sensor in combination with the memristor constitutes a neurotransmitter-mediated artificial synapse, as shown in Fig. 11(c), which enables both neurotransmitter recognition and memory capabilities. To verify the perceptual memory ability, different concentrations of DA were used as presynaptic stimuli, and the electrical response of the artificial synapse was monitored. After stimulation with a low concentration of 10 μM DA, the sensor current increased to 5.21 μA, as shown in Fig. 11(d). The current change of the memristor was negligible, indicating that the low concentration of DA was unable to form Ag-conducting filaments (CFs) in it. When the DA concentration was increased to 40 μM, the sensor current rose to 22.82 μA, and the memristor current also increased. Upon removing the DA stimulus, the memristor current returned to the high-resistance state (HRS), implying that moderate DA signals induced STP (short-term plasticity) behaviors and the formation of unstable CFs in the memristor. When the DA concentration was further increased to 200 μM, both the memristor and sensor currents increased in parallel. The current does not return to HRS even when DA is removed, indicating that the memristor undergoes LTP behavior under high DA concentration stimulation, accompanied by the formation of a stable CF internally.

This low-resistance state (LRS) induced by strong DA stimulation can subsequently trigger the release of DA, sending out artificial neuronal electrical discharge signals. To mimic interneurons, DA sensors, memristors, and thermo-responsive DA hydrogels were integrated to perform or exhibit pre-neurotransmitter recognition, synaptic plasticity, and post-neurotransmitter release functions, respectively, as shown in Fig. 11(e). PDMS-based microfluidic channels were integrated with the chip to implement the flow of neurotransmitters. The inset of Fig. 11(f) shows the integrated chip. When the concentration of DA was gradually increased from 0 to 50 μM, the sensor response and hydrogel release were monitored, as shown in Fig. 11(f). To visualize the flow of hydrogel release in microfluidics, methyl blue was encapsulated in a hydrogel, as shown in Fig. 11(g). When a continuous DA stimulus of 20 μM was applied, a continuous flow of the dye solution into the microfluidic channel was observed—confirming the stimulus-triggered release behavior. This process mimics the excitation of action potentials and the release of neurotransmitters into the synaptic gap of biological neurons, thereby forming a chemical communication circuit that is analogous to the one found in interneurons. Liu et al. present a memristor-based neural signal analysis system that leverages the biologically plausible properties of memristors to efficiently analyze analog signals.[141] To demonstrate the system's proof-of-concept, an array of memristors is used to enable the filtering and identification of epileptic signals. Specifically, the authors constructed a memristor-based FIR filter as a preprocessor; and a memristor-based single-layer perceptron neural network as a decoder—to perform the typical BMI task of identifying epilepsy-related brain states from recorded neural signals, as shown in Fig. 12(a). Frequency-dependent information in neural signals aids in distinguishing between different brain states. Therefore, a FIR filter array with four bands of bass filters was designed and implemented using memristors to generate waveforms in the corresponding frequency bands, as shown in Fig. 12(a). Fig. 12(b) shows how the neural signal is filtered in the memristor array. The coefficients of the filter are first mapped onto the memristor array as device conductance values. Fragments of analogue voltage signals containing information about the state of the brain (i.e., normal, interictal, or ictal) are then applied to the memristor array. The sum of the output currents is the result of filtering by the filter bank at each time step. In this way, the memristor array filters the input neural signal into four frequency bands (δ, θ, α, and β) with waveforms reflecting the corresponding brain states. Several biomarkers, such as waveform amplitude and energy per frequency band, were subsequently extracted as feature parameters and input into a single-layer perceptron neural network to identify epilepsy-related brain states. To verify that the filtering results retained sufficient information for identifying brain states, the authors further constructed a single-layer perceptron neural network consisting of 21 input neurons, with output neurons located in another array of memristors. To compare the performance of software computation with that of the memristor-based filter set, the authors created two datasets: dataset S, consisting of all biomarkers extracted from software computation results, and dataset M, consisting of all biomarkers extracted from the filtered waveforms of the memristor array. Fig. 12(c) shows the input feature vectors for the 540 test samples. The conductance map of the neural network based on the memristor array, using 126 devices for 63 synapses with differential weights and trained by dataset M, is shown in Fig. 12(d). Fig. 12(e) displays the output values for the 540 test samples. The identification accuracies of the neural

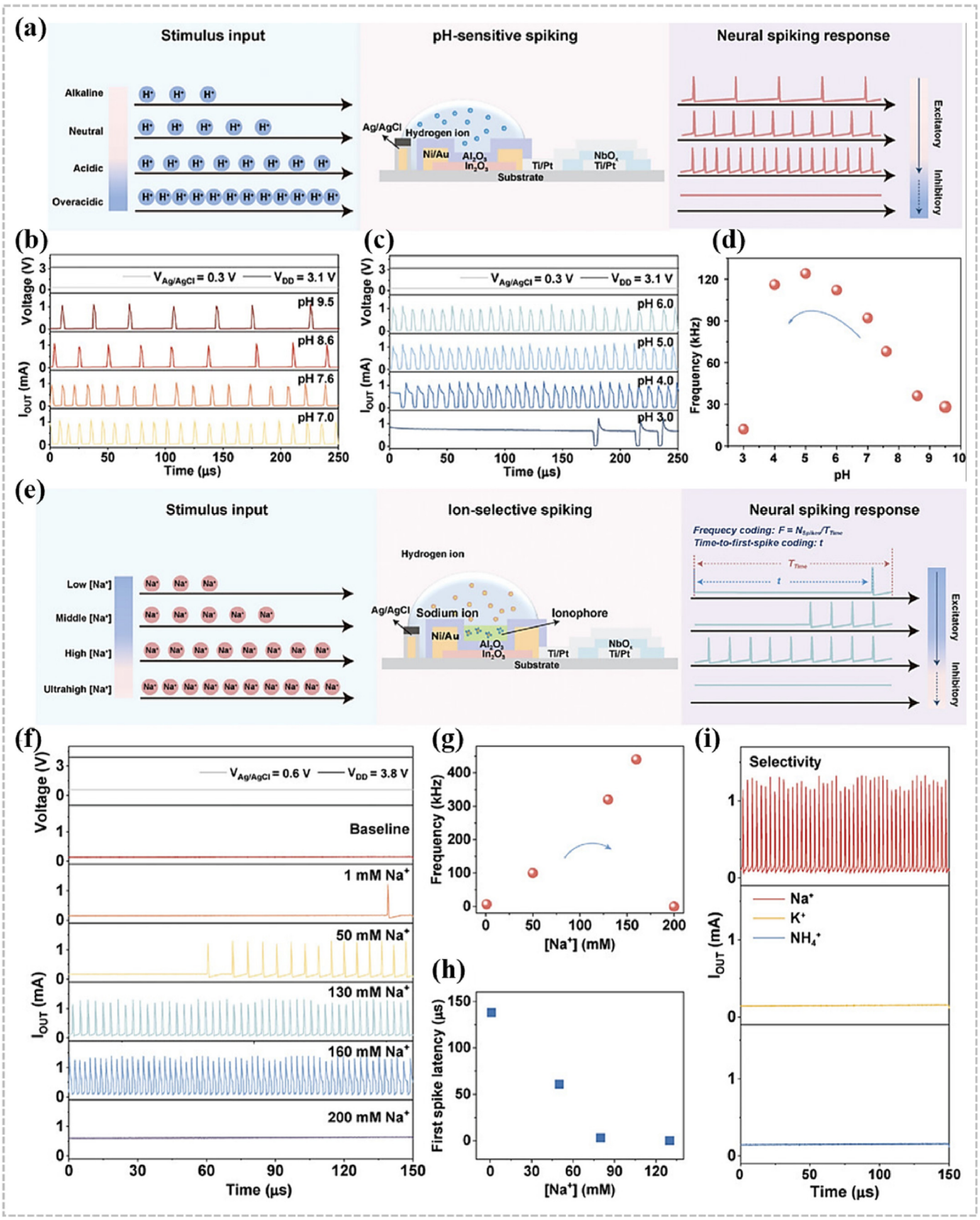

(caption on next page)

Fig. 13. (a) The schematic representation of the stimulus–response model of a pH-sensitive SCN, wherein the presence of hydrogen ions elicits oscillatory spiking behavior characterized by pH levels. The substrate refers to Si/SiO_2. The depicted device mirrors the excitatory and inhibitory phenomena akin to biological neurons, illustrating the nuanced dynamics of pH-induced spiking behaviors within the SCN. (b) and (c) The current spiking characteristics (I_{OUT}–t) for various pH ranging from 3 to 10, showing spiking current patterns of a pH-sensitive SCN in both alkaline and acidic environments. The spiking frequency exhibits an ascending trend in alkaline conditions. Conversely, within an acidic milieu, the frequency initially rises, followed by a subsequent decrease correlated with the ascending concentration of H+. (d) The frequency response corresponding to different pH levels. (e) The schematic depiction of the stimulus–response model of an ion-selective SCN, specifically responsive to the Na + concentration. The substrate refers to Si/SiO_2. The Na^+ -selective SCN exhibits oscillatory spiking behavior, characterized by Na^+ levels. The device shows the integration of both frequency coding and TTFS coding mechanisms, mirroring the modulation induced by Na+. T_{Time} represents the time window of the programmed measurement. The TTFS time, denoted as t, is measured as the time interval between the onset of the stimulus and the occurrence of the first spike. (f) The representative spiking firing behavior of the Na + -selective SCN across various Na^+ concentrations. The spiking frequency initially demonstrates a monotonic increase, ranging from 7 to 439 kHz, with an improvement in Na^+ concentration from 1 to 160 × 10^{-3} m. However, upon further elevation to 200 × 10^{-3} m Na^+, the spiking frequency declines to 0 Hz. (g) Spiking frequency as a function of the various ion concentrations for Na + -selective SCN. (h) The TTFS coding from 138 to 3 μs with an increase in Na + concentration from 1 to 160 × 10^{-3} m in Na + -selective SCN. (i) Ion-selective SCN inducing ion-specific oscillations, which produce spikes exclusively in Na^+ solution but not in K^+ or NH_4^+ solutions. Copyright 2024, Wiley-VCH GmbH.[143].

networks with software-trained weights using dataset S (S.S.), software-trained weights using dataset M (M.S.), and experimentally mapped weights after training on dataset M (M.M.) are compared in Fig. 12(f).

It can be observed that the accuracy of the M.S. simulation is almost the same as the S.S. simulation. This result confirms that the filter bank based on the memristor array retains sufficient recognition information and performs as well as the software implementation. In contrast, the M.M. experimental results show a slight decrease in accuracy, which can be attributed to the non-ideal device characteristics of the memristor array. It is expected that this problem can be mitigated by using larger neural networks or adopting new training strategies. In addition to achieving high accuracy, the memristor-based analogue computing system offers an attractive platform for designing low-power, high-efficiency BMI neural signal analysis systems. To compare the performance of the memristor-based system with that of a state-of-the-art CMOS-based ASIC, the authors evaluated the power efficiencies of both systems, as shown in Fig. 12(g). The memristor array-based system achieves an excellent power efficiency of 1.4 μW/level, where most of the power is consumed by the filter bank due to the relatively small size of the perceptron network used for recognition. In comparison, the power efficiency of a typical CMOS system is estimated to be 551.0 μW/level. Thus, compared to state-of-the-art CMOS systems, memristor-based systems exhibit an approximately 400-fold advantage in power efficiency. These unique advantages render memristor arrays an attractive candidate for future high-throughput analogue neural signal analysis in fully implanted BMIs.

In addition to transmitting information, brain-computer interfaces and implantable devices need to be able to interpret and transmit basic chemical and physiological signals from humans to computers.[142] This ability can restore or enhance bodily functions related to sensation, movement and control. To address this challenge, hardware-based neuromorphic devices have emerged to provide brain-like, energy-efficient solutions for processing biological signals. Zhu et al. report a bio-integrated spiking chemical neuron (SCN) that implements ion-mediated spiking behavior via an oxide field-effect transistor (FET)-type chemical sensor and a niobium oxide Mott memristor.[143] Initially, the authors investigated pH-mediated spiking in SCN, where an Al_2O_3/In_2O_3-based FET sensor was used as the pH-sensitive element. Fig. 13(a) illustrates a schematic of the pH response model characterizing pH-sensitive SCNs, where different H^+ concentrations can trigger different spiking patterns in SCNs. Fig. 13(b) and (c) further explore the behavior of the pH-sensitive SCN. Under alkaline conditions, there is a clear trend of increasing spike frequency. In contrast, in acidic environments, the frequency decreases after an initial rise, and these fluctuations are closely correlated with the rising H^+ concentration. Fig. 13(d) shows the highest spike frequency (125 kHz) observed at pH = 5.0, which indicates a critical point for the modulation of neuron-like spiking behavior. Thus, the prepared SCN can achieve excitatory and inhibitory behaviors under the modulation of H^+, reflecting the subtle dynamics inherent in biological neurons. In addition, by modifying the field effect transistor sensor with an ion-selective ionophore, the SCN can realize spiking pulses mediated by Na^+, as shown in Fig. 13(e). The authors investigated the spiking dynamics of SCN at different Na + concentrations. Fig. 13(f) demonstrates the spiking pattern of Na^+ selective SCN at different concentrations. As the Na+ concentration increases from 1 to 160 × 10^{-3} M, the spike frequency shows a monotonic increase. However, when the Na + concentration was increased further to 200 × 10^{-3} M, the spiking ceased, which resembles the excitatory and inhibitory properties of biological neurons. Under the 130 × 10^{-3} M Na^+ condition, the peak energy consumption of SCN was about 3.4 nJ per spike, as shown in Fig. 13(g). Interestingly, as shown in Fig. 13(h), a stimulus-response spike latency was observed in the Na^+-selective SCN, similar to the TTFS encoding in biological neurons. Fig. 13(i) demonstrates the spike current of SCN in different solutions. It produces spike currents only in Na^+ solution and not in K^+ or NH_4^+ solution, which indicates that SCN shows high Na^+ selectivity. The ion-mediated SCN offers a pathway to emulate the spiking dynamics of biological neurons in a manner that is more biologically plausible. Neuromorphic devices face multifaceted biotechnological challenges in brain-computer interface applications: implantable systems suffer from impedance drift induced by electrodes, which continuously degrades precision, while mechanical rigidity mismatches with cortical tissue provoke chronic inflammatory responses. Non-invasive systems circumvent surgical risks yet face signal dispersion limitations. Furthermore, emerging neurochemical coupling interfaces reveal critical limitations—the neurotransmitter regulation cycle lags behind biological neural conduction rates, and a lack of dynamic regulatory mechanisms for electrochemical-pulse signal coordination severely constrains closed-loop adaptability in brain-machine symbiotic systems.

5. Summary and outlook

In summary, this paper focuses on the application of neuromorphic devices in biomedical engineering and provides a comprehensive overview of the latest research results and developments in this field. Firstly, this study summarizes and analyzes in depth the pathogenesis of diseases affecting different parts of the human body and their conventional/novel detection methods. The core aim is to comprehensively analyze the potential root causes of these diseases and to provide useful references for medical research and clinical practice. The article then reviews the wide range of applications of neuromorphic devices in the field of biomedical sensing technology and the remarkable results they have achieved. Thanks to their unique neuromorphic structure, these devices have exhibited exceptional ability to accurately capture biological signals, thereby providing powerful technical support for biomedical research. Additionally, this paper delves into the application prospects of neuromorphic devices in the field of medical image processing. By processing and analyzing various common medical image types, including X-rays, MRI, CT, and others, neuromorphic devices demonstrate great potential in medical image recognition, diagnosis, and assisted treatment. Meanwhile, this review underscores the innovative applications of

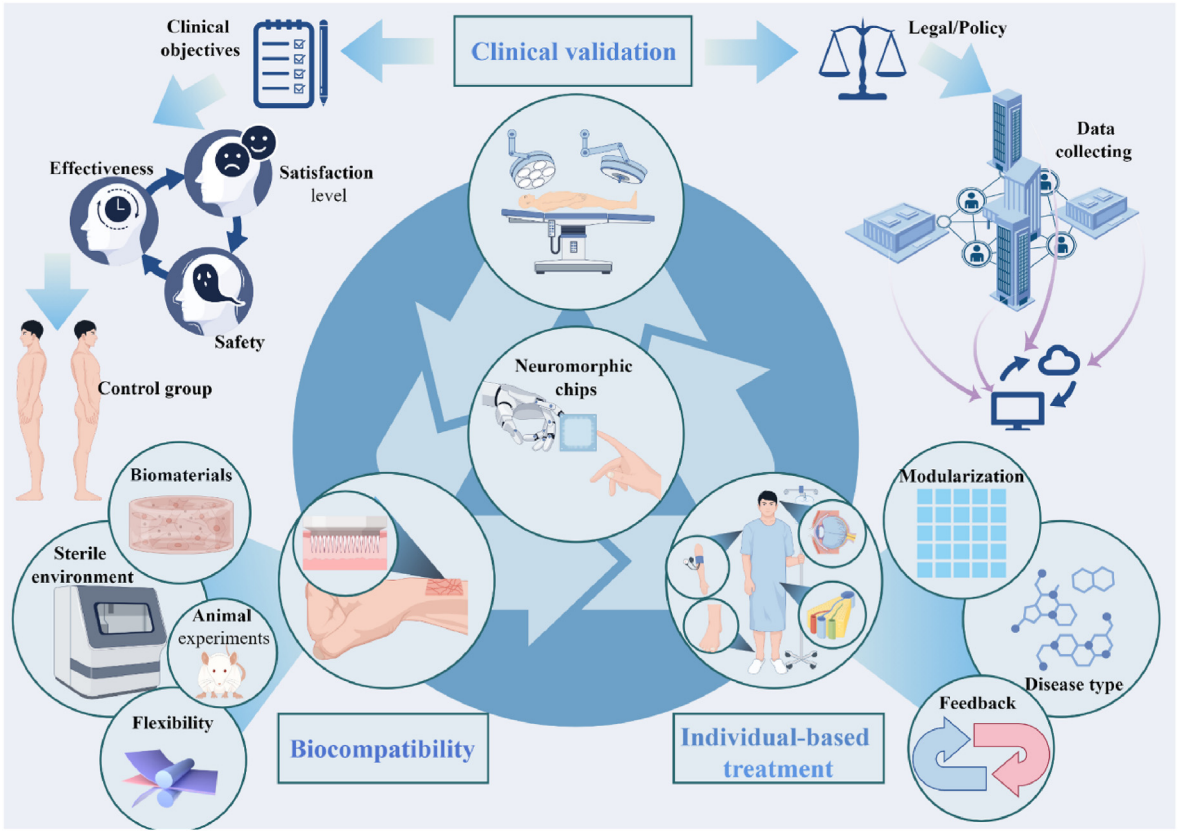

Fig. 14. The research line of neuromorphic chips in the field of biomedical engineering includes three aspects: biocompatibility, Individual-based treatment and clinical validation. The figure was drawn by Figdraw.

neuromorphic devices in rehabilitation medical engineering and the breakthroughs they have accomplished. Notably, in the areas of afferent neural network construction and e-skin design, neuromorphic devices have infused new vitality into the progress of rehabilitation medical engineering, leveraging their unique advantages to provide more precise and efficient solutions for patients' rehabilitation treatment and functional recovery. Finally, the article also comprehensively examines the latest research findings and development trends of neuromorphic devices in the fields of neuroscience and brain-computer interfaces. These studies have demonstrated that neuromorphic devices possess significant potential for achieving seamless connections between the brain and external devices. They offer new insights and directions for neuroscience research, the advancement of brain-computer interface technology, and future innovations in human-computer interaction. Furthermore, all these studies indicate that neuromorphic devices exhibit lower power consumption and higher performance compared to conventional electronic devices. This renders them more promising for a broader range of applications in biomedical engineering, particularly in scenarios that necessitate prolonged monitoring and treatment. The low power consumption aids in extending the device's lifespan while minimizing disruption to the patient's daily life. The research of neuromorphic devices in the field of biomedical engineering has made great progress. However, with the improvement of people's living standards and medical needs, as well as the increasing importance of cross-disciplinary disciplines such as biomedical engineering, the development of neuromorphic devices is still faced with many challenges, including device biocompatibility, personalized demand handling, and clinical validation, which urgently require further in-depth research and solutions(Fig. 14).[144,145]

(1) Biocompatibility refers to the ability of biomaterials to come into contact with living biological tissues and body fluids without causing a decline in the function of cells and tissues, or inducing inflammation, cancerous changes, rejection reactions, and other adverse effects.[146,147] In biomedical engineering, the biocompatibility of neuromorphic devices is crucial for their successful clinical application. To reduce the occurrence of immune reactions and rejection, materials with excellent biocompatibility are selected. Emerging generative AI models are accelerating this process by predicting novel biocompatible material combinations through multi-parameter optimization of chemical properties and biological interaction profiles. The surface of neuromorphic devices is modified using chemical, physical, or biological methods to enhance their compatibility with biological tissues. Additionally, flexible materials and techniques can be employed to design neuromorphic devices that possess flexibility. Such designs can better accommodate morphological changes in biological tissues and minimize damage and discomfort during implantation, thereby improving the biocompatibility of the devices. Furthermore, during the preparation process, researchers must strictly control the experimental environment to ensure the sterile fabrication of neuromorphic devices. This helps to decrease the risk of infection after implantation and further enhances biocompatibility. By integrating these approaches, the widespread adoption of neuromorphic devices in biomedical engineering can be facilitated, thereby making a significant contribution to the advancement of the medical field.

(2) In the field of biomedical engineering, personalized needs pertain to the characteristics of a treatment plan or rawmedical device that is tailored to each patient based on factors such as individual differences, physiological status, disease type, and severity.[148] This concept of customization aims to maximize treatment effectiveness, minimize side effects, and enhance the quality of life and satisfaction of patients. For neuromorphic devices, enhancing

their ability to meet patients' personalized needs entails not only considering the functionality and biocompatibility of the device, but also accounting for the specific conditions of the patient to achieve precision medicine. AI-powered digital twin technology creates patient-specific physiological models to simulate device performance, enabling virtual prototyping of customized neuromorphic solutions before physical implantation. First, a modular design concept is adopted, allowing the functions of each part of the neuromorphic device to be replaced or upgraded independently. In this manner, doctors can flexibly select or adjust the functional modules of the device according to the patient's specific conditions, thereby achieving a more personalized treatment plan. Second, an effective patient feedback mechanism is established, incorporating information such as pain perception. This information is crucial for adjusting the design, function, and parameters of the neuromorphic device, enabling the achievement of customized treatments that are even more tailored to the patient's needs.

(3) Clinical validation is the systematic and scientific evaluation of a treatment, medical device, or drug to determine its safety, efficacy, and applicability in medical research and clinical practice. For neuromorphic devices, clinical validation is a critical step to ensure their safe and effective use in biomedical engineering. Based on the intended use and performance characteristics of the neuromorphic device, the objectives of clinical validation are clearly defined, including assessing the device's safety, efficacy, stability, and patient acceptance. AI-driven predictive modeling significantly enhances trial design efficiency by identifying optimal patient cohorts and predicting potential adverse event probabilities through retrospective analysis of historical medical datasets. Collect basic patient data and follow up on treatment outcomes and patient feedback after the neuromorphic device is used. Establish a control group to compare patients using the neuromorphic device with those not using it, in order to assess the therapeutic effect of the device. Conduct clinical validation in various medical centers to expand the sample size and enhance the representativeness and credibility of the validation results. A comprehensive data collection system should also be established to ensure the completeness, accuracy, and traceability of the data. This system should include the collection of patients' baseline data, physiological indicators during treatment, imaging results, and patients' subjective feedback. Meanwhile, researchers need to refer to relevant regulations, guidelines, and standards both domestically and internationally to formulate clinical validation criteria and evaluation indexes for neuromorphic devices. Through the comprehensive application of these methods, the safety and effectiveness of neuromorphic devices in clinical applications can be ensured, thereby promoting their widespread application and development in the field of biomedical engineering.

CRediT authorship contribution statement

Kaiyang Wang: Writing – original draft, Data curation, Conceptualization. **Shuhui Ren:** Writing – original draft, Investigation, Data curation. **Yunfang Jia:** Writing – review & editing, Investigation. **Xiaobing Yan:** Writing – review & editing, Supervision. **Lizhen Wang:** Writing – review & editing, Project administration, Funding acquisition. **Yubo Fan:** Writing – review & editing, Project administration.

Ethical approval

This study does not contain any studies with human or animal subjects performed by any of the authors.

Declaration of competing interests

The authors declare no interest conflict. They have no known competing financial interests or personal relationships that could influence the work reported in this paper.

Funding and Acknowledgements

This work was supported by the National Science Foundation for Distinguished Young Scholars of China (Grant No. 12425209), the National Natural Science Foundation of China (11827803, 12172034, 62004056, 62104058, 62271269).

References

1. Hong G, Antaris AL, Dai H. Near-infrared fluorophores for biomedical imaging. *Nat Biomed Eng*. 2017;1(1):10.
2. Won SM, Cai L, Gutruf P, Rogers JA. Wireless and battery-free technologies for neuroengineering. *Nat Biomed Eng*. 2023;7(4):405–423.
3. Cook JA, Shah KB, Quader MA, et al. The total artificial heart. *J Thorac Dis*. 2015; 7(12):2172.
4. Pattichis CS, Kyriacou E, Voskarides S, Pattichis MS, Istepanian R, Schizas CN. Wireless telemedicine systems: an overview. *IEEE Antenn Propag Mag*. 2002;44(2): 143–153.
5. Hinde K, White G, Armstrong N. Wearable devices suitable for monitoring twenty four hour heart rate variability in military populations. *Sensors*. 2021;21(4):1061.
6. Lee H, Song C, Hong YS, et al. Wearable/disposable sweat-based glucose monitoring device with multistage transdermal drug delivery module. *Sci Adv*. 2017;3(3):1601314.
7. Guk K, Han G, Lim J, et al. Evolution of wearable devices with real-time disease monitoring for personalized healthcare. *Nanomaterials*. 2019;9(6):813.
8. Jacobi A, Chung M, Bernheim A, Eber C. Portable chest X-ray in coronavirus disease-19 (COVID-19): a pictorial review. *Clin Imag*. 2020;64:35–42.
9. Davis GR, Wong FS. X-ray microtomography of bones and teeth. *Physiol Meas*. 1996; 17(3):121.
10. Zhao B, Li T, Fan Z, et al. Heart-brain connections: phenotypic and genetic insights from magnetic resonance images. *Science*. 2023;380(6648):abn6598.
11. Wang L, Wu M, Li R, Xu X, Zhu C, Feng X. MVI-mind: a novel deep-learning strategy using computed tomography (CT)-based radiomics for end-to-end high efficiency prediction of microvascular invasion in hepatocellular carcinoma. *Cancers*. 2022; 14(12):2956.
12. Razzak MI, Naz S, Zaib A. *Deep learning for medical image processing: overview, challenges and the future. Classification in BioApps: Automation of Decision Making*. 2018:323–350.
13. Roth HR, Shen C, Oda H, et al. Deep learning and its application to medical image segmentation. *Med imaging Technol*. 2018;36(2):63–71.
14. Wang K, Ren S, Jia Y, Yan X. Dual biological-clock controllable low-power fibrous synapse array based on heterojunction switched conductive filaments. *Nano Energy*. 2024;127:109765.
15. Yan X, Wang K, Zhao J, et al. A new memristor with 2D Ti3C2Tx MXene flakes as an artificial bio-synapse. *Small*. 2019;15(25):1900107.
16. Yan X, Zhao J, Liu S, et al. Memristor with Ag-cluster-doped TiO2 films as artificial synapse for neuroinspired computing. *Adv Funct Mater*. 2018;28(1):1705320.
17. Zhang X, Zhuo Y, Luo Q, et al. An artificial spiking afferent nerve based on Mott memristors for neurorobotics. *Nat Commun*. 2020;11(1):51.
18. Zhu J, Wang Z, Liu D, et al. Flexible low-voltage MXene floating-gate synaptic transistor for neuromorphic computing and cognitive learning. *Adv Funct Mater*. 2024:2403842.
19. Zhou F, Chai Y. Near-sensor and in-sensor computing. *Nat. Electron.* 2020;3(11): 664–671.
20. Wang K, Hu Q, Gao B, et al. Threshold switching memristor-based stochastic neurons for probabilistic computing. *Mater Horiz*. 2021;8(2):619–629.
21. Yao P, Wu H, Gao B, et al. Fully hardware-implemented memristor convolutional neural network. *Nature*. 2020;577(7792):641–646.
22. Aguirre F, Sebastian A, Le Gallo M, et al. Hardware implementation of memristor-based artificial neural networks. *Nat Commun*. 2024;15(1):1974.
23. Tan D, Sun N, Huang J, et al. Monolayer vacancy-induced MXene memory for write-verify-free programming. *Small*. 2024:2402273.
24. Tan D, Zhang Z, Shi H, et al. Bioinspired artificial visual-respiratory synapse as multimodal scene recognition system with oxidized-vacancies MXene. *Adv Mater*. 2024;36(36):2407751.
25. Wang K, Li L, Zhao R, et al. A pure 2H-MoS2 nanosheet-based memristor with low power consumption and linear multilevel storage for artificial synapse emulator. *Advanced Electronic Materials*. 2020;6(3):1901342.
26. Zhang T, Cheng X, Jia S, Poo M-m, Zeng Y, Xu B. Self-backpropagation of synaptic modifications elevates the efficiency of spiking and artificial neural networks. *Sci Adv*. 2021;7(43):0146.
27. Sun C, Sun H, Xu J, et al. An energy efficient STDP-based SNN architecture with on-chip learning. *IEEE Transactions on Circuits and Systems I: Regular Papers*. 2022; 69(12):5147–5158.

28. Sharma D, Rath SP, Kundu B, et al. Linear symmetric self-selecting 14-bit kinetic molecular memristors. *Nature*. 2024;633(8030):560–566.
29. Soni S, Ruhela RK, Medhi B. Nanomedicine in central nervous system (CNS) disorders: a present and future prospective. *Adv Pharmaceut Bull*. 2016;6(3):319.
30. Ghose AK, Herbertz T, Hudkins RL, Dorsey BD, Mallamo JP. Knowledge-based, central nervous system (CNS) lead selection and lead optimization for CNS drug discovery. *ACS Chem Neurosci*. 2012;3(1):50–68.
31. Wraith DC, Nicholson LB. The adaptive immune system in diseases of the central nervous system. *J Clin Investig*. 2012;122(4):1172–1179.
32. Kesselheim AS, Hwang TJ, Franklin JM. Two decades of new drug development for central nervous system disorders. *Nat Rev Drug Discov*. 2015;14(12):815.
33. Thijs RD, Surges R, O'Brien TJ, Sander JW. Epilepsy in adults. *The lancet*. 2019; 393(10172):689–701.
34. Pandolfo M. *Genetics of Epilepsy*. © Thieme Medical Publishers; 2011:506–518.
35. Richardson MP. Large scale brain models of epilepsy: dynamics meets connectomics. *J Neurol Neurosurg Psychiatr*. 2012;83(12):1238–1248.
36. Lowenstein DH. Epilepsy after head injury: an overview. *Epilepsia*. 2009;50:4–9.
37. Smith SJ. EEG in the diagnosis, classification, and management of patients with epilepsy. *J Neurol Neurosurg Psychiatr*. 2005;76(Suppl 2):2–7.
38. Noachtar S, Rémi J. The role of EEG in epilepsy: a critical review. *Epilepsy Behav*. 2009;15(1):22–33.
39. Wang ZI, Alexopoulos AV, Jones SE, Jaisani Z, Najm IM, Prayson RA. The pathology of magnetic-resonance-imaging-negative epilepsy. *Mod Pathol*. 2013;26(8): 1051–1058.
40. Stelzle D, Schmidt V, Keller L, et al. Characteristics of people with epilepsy and Neurocysticercosis in three eastern African countries–A pooled analysis. *PLoS Neglected Trop Dis*. 2022;16(11):e0010870.
41. Poewe W, Seppi K, Tanner CM, et al. Parkinson disease. *Nat Rev Dis Primers*. 2017; 3(1):1–21.
42. Armstrong MJ, Okun MS. Diagnosis and treatment of Parkinson disease: a review. *JAMA*. 2020;323(6):548–560.
43. Dickson DW. Neuropathology of Parkinson disease. *Park Relat Disord*. 2018;46: S30–S33.
44. Kaveh R, Schwendeman C, Pu L, Arias AC, Muller R. Wireless ear EEG to monitor drowsiness. *Nat Commun*. 2024;15(1):6520.
45. Hoffman JI, Kaplan S. The incidence of congenital heart disease. *J Am Coll Cardiol*. 2002;39(12):1890–1900.
46. Maron BJ, Maron MS. Hypertrophic cardiomyopathy. *Lancet*. 2013;381(9862): 242–255.
47. Glantz SA, Parmley WW. Passive smoking and heart disease: mechanisms and risk. *JAMA*. 1995;273(13):1047–1053.
48. Day E, Rudd JH. Alcohol use disorders and the heart. *Addiction*. 2019;114(9): 1670–1678.
49. Willett WC. Dietary fats and coronary heart disease. *J Intern Med*. 2012;272(1): 13–24.
50. Marijon E, Mirabel M, Celermajer DS, Jouven X. Rheumatic heart disease. *Lancet*. 2012;379(9819):953–964.
51. Auer R, Bauer DC, Marques-Vidal P, et al. Association of major and minor ECG abnormalities with coronary heart disease events. *JAMA*. 2012;307(14): 1497–1505.
52. Archbold RA, Robinson NM, Schilling RJ. Radial artery access for coronary angiography and percutaneous coronary intervention. *Bmj*. 2004;329(7463): 443–446.
53. Gill SK, Barsky A, Guan X, et al. Consumer wearable devices for evaluation of heart rate control using digoxin versus beta-blockers: the RATE-AF randomized trial. *Nat Med*. 2024;30(7):2030–2036.
54. Hu H, Huang H, Li M, et al. A wearable cardiac ultrasound imager. *Nature*. 2023; 613(7945):667–675.
55. Alanee S, McGee L, Jackson D, et al. Association of serotypes of Streptococcus pneumoniae with disease severity and outcome in adults: an international study. *Clin Infect Dis*. 2007;45(1):46–51.
56. Kahl BC. Impact of Staphylococcus aureus on the pathogenesis of chronic cystic fibrosis lung disease. *International Journal of Medical Microbiology*. 2010;300(8): 514–519.
57. Ruuskanen O, Lahti E, Jennings LC, Murdoch DR. Viral pneumonia. *Lancet*. 2011; 377(9773):1264–1275.
58. Qi X-M, Luo Y, Song M-Y, et al. Pneumoconiosis: current status and future prospects. *Chinese medical journal*. 2021;134(8):898–907.
59. Collins J. CT signs and patterns of lung disease. *Radiol Clin*. 2001;39(6):1115–1135.
60. Biederer J, Mirsadraee S, Beer M, et al. MRI of the lung (3/3)—current applications and future perspectives. *Insights into imaging*. 2012;3:373–386.
61. Zhao Y, Ding Y, Lau V, et al. Whole-body magnetic resonance imaging at 0.05 Tesla. *Science*. 2024;384(6696):eadm7168.
62. Seo G, Lee G, Kim MJ, et al. Rapid detection of COVID-19 causative virus (SARS-CoV-2) in human nasopharyngeal swab specimens using field-effect transistor-based biosensor. *ACS Nano*. 2020;14(4):5135–5142.
63. Kwon K, Kim JU, Won SM, et al. A battery-less wireless implant for the continuous monitoring of vascular pressure, flow rate and temperature. *Nat Biomed Eng*. 2023; 7(10):1215–1228.
64. Zhou S, Gao X, Park G, et al. Transcranial volumetric imaging using a conformal ultrasound patch. *Nature*. 2024;629(8013):810–818.
65. Gao X, Chen X, Lin M, et al. A wearable echomyography system based on a single transducer. *Nat. Electron.* 2024:1–12.
66. Xu C, Song Y, Sempionatto JR, et al. A physicochemical-sensing electronic skin for stress response monitoring. *Nat. Electron.* 2024;7(2):168–179.
67. Court-Brown CM, Caesar B. Epidemiology of adult fractures: a review. *Injury*. 2006; 37(8):691–697.
68. Rachner TD, Khosla S, Hofbauer LC. Osteoporosis: now and the future. *Lancet*. 2011;377(9773):1276–1287.
69. Al-Ayyoub M, Hmeidi I, Rababah H. Detecting hand bone fractures in X-ray images. *J Multim Process Technol*. 2013;4(3):155–168.
70. Hopper RA, Salemy S, Sze RW. Diagnosis of midface fractures with CT: what the surgeon needs to know. *Radiographics*. 2006;26(3):783–793.
71. Nachtrab O, Cassar-Pullicino V, Lalam R, Tins B, Tyrrell P, Singh J. Role of MRI in hip fractures, including stress fractures, occult fractures, avulsion fractures. *Eur J Radiol*. 2012;81(12):3813–3823.
72. Dawson AL, Dellavalle RP, Elston DM. Infectious skin diseases: a review and needs assessment. *Dermatol Clin*. 2012;30(1):141–151.
73. Fonacier LS, Dreskin SC, Leung DY. Allergic skin diseases. *J Allergy Clin Immunol*. 2010;125(2):S138–S149.
74. Burks W. Skin manifestations of food allergy. *Pediatrics*. 2003;111:1617–1624.
75. Taketomi EA, Sopelete MC, Moreira PFdS, Vieira FdAM. Pollen allergic disease: pollens and its major allergens. *Rev Bras Otorrinolaringol*. 2006;72:562–567.
76. Borchers AT, Naguwa SM, Shoenfeld Y, Gershwin ME. The geoepidemiology of systemic lupus erythematosus. *Autoimmun Rev*. 2010;9(5):A277–A287.
77. Merin K, Shaji M, Kameswaran R. A review on sun exposure and skin diseases. *Indian J Dermatol*. 2022;67(5):625.
78. Kaliyadan F. The scope of the dermoscope. *Indian Dermatology Online Journal*. 2016; 7(5):359–363.
79. Elston DM, Stratman EJ, Miller SJ. Skin biopsy: biopsy issues in specific diseases. *J Am Acad Dermatol*. 2016;74(1):1–16.
80. Conti-Fine BM, Milani M, Kaminski HJ. Myasthenia gravis: past, present, and future. *J Clin Investig*. 2006;116(11):2843–2854.
81. Farrugia ME, Di Marco M, Kersel D, Carmichael C. A physical and psychological approach to managing fatigue in myasthenia gravis: a pilot study. *J Neuromuscul Dis*. 2018;5(3):373–385.
82. Abramsky O, Aharonov A, Teitelbaum D, Fuchs S. Myasthenia gravis and acetylcholine receptor: effect of steroids in clinical course and cellular immune response to acetylcholine receptor. *Arch Neurol*. 1975;32(10):684–687.
83. Chiou-Tan FY, Gilchrist JM. Repetitive nerve stimulation and single-fiber electromyography in the evaluation of patients with suspected myasthenia gravis or Lambert–Eaton myasthenic syndrome: review of recent literature. *Muscle Nerve*. 2015;52(3):455–462.
84. Peeler CE, De Lott LB, Nagia L, Lemos J, Eggenberger ER, Cornblath WT. Clinical utility of acetylcholine receptor antibody testing in ocular myasthenia gravis. *JAMA Neurol*. 2015;72(10):1170–1174.
85. Abella V, Scotece M, Conde J, et al. Leptin in the interplay of inflammation, metabolism and immune system disorders. *Nat Rev Rheumatol*. 2017;13(2):100–109.
86. Delves PJ, Roitt IM. The immune system. *N Engl J Med*. 2000;343(1):37–49.
87. Tecklenborg J, Clayton D, Siebert S, Coley S. The role of the immune system in kidney disease. *Clin Exp Immunol*. 2018;192(2):142–150.
88. McCarthy CE, White JM, Viola NT, Gibson HM. In vivo imaging technologies to monitor the immune system. *Front Immunol*. 2020;11:1067.
89. Nichol ST, Arikawa J, Kawaoka Y. Emerging viral diseases. *Proc Natl Acad Sci*. 2000; 97(23):12411–12412.
90. Indiveri G, Douglas R. Neuromorphic vision sensors. *Science*. 2000;288(5469): 1189–1190.
91. Robilotti E, Deresinski S, Pinsky BA. Norovirus. *Clin Microbiol Rev*. 2015;28(1): 134–164.
92. Li X, Wang J, Geng J, Xiao L, Wang H. Emerging landscape of SARS-CoV-2 variants and detection technologies. *Mol Diagn Ther*. 2023;27(2):159–177.
93. Kukar M, Gunčar G, Vovko T, et al. COVID-19 diagnosis by routine blood tests using machine learning. *Sci Rep*. 2021;11(1):10738.
94. Wang K, Jia Y, Yan X. Neuro-receptor mediated synapse device based on crumpled MXene $Ti_3C_2T_x$ nanosheets. *Adv Funct Mater*. 2021;31(48).
95. Zhai Y, Zhou Y, Yang X, et al. Near infrared neuromorphic computing via upconversion-mediated optogenetics. *Nano Energy*. 2020;67doi. https://doi.org/10.1016/j.nanoen.2019.104262.
96. Zhou L, Yang S, Ding G, et al. Tunable synaptic behavior realized in C3N composite based memristor. *Nano Energy*. 2019;58:293–303.
97. Strukov DB, Snider GS, Stewart DR, Williams RS. The missing memristor found. *Nature*. 2008;453(7191):80–83.
98. Jo SH, Chang T, Ebong I, Bhadviya BB, Mazumder P, Lu W. Nanoscale memristor device as synapse in neuromorphic systems. *Nano Lett*. 2010;10(4):1297–1301.
99. Wang M, Cai S, Pan C, et al. Robust memristors based on layered two-dimensional materials. *Nat. Electron.* 2018;1(2):130–136.
100. Huang H, Liang X, Wang Y, et al. Fully integrated multi-mode optoelectronic memristor array for diversified in-sensor computing. *Nat Nanotechnol*. 2024:1–11.
101. Diorio C, Hasler P, Minch A, Mead CA. A single-transistor silicon synapse. *IEEE Trans Electron Dev*. 1996;43(11):1972–1980.
102. Lai Q, Zhang L, Li Z, Stickle WF, Williams RS, Chen Y. Ionic/electronic hybrid materials integrated in a synaptic transistor with signal processing and learning functions. *Adv Mater*. 2010;22(22):2448–2453.
103. Yang CS, Shang DS, Liu N, et al. A synaptic transistor based on quasi-2D molybdenum oxide. *Adv Mater*. 2017;29(27):1700906.
104. Cui J, An F, Qian J, et al. CMOS-compatible electrochemical synaptic transistor arrays for deep learning accelerators. *Nat. Electron.* 2023;6(4):292–300.
105. Lee HR, Lee D, Oh JH. A hippocampus-inspired dual-gated organic artificial synapse for simultaneous sensing of a neurotransmitter and light. *Adv Mater*. 2021;33(17): 2100119.

106. Wang K, Dai S, Zhao Y, Wang Y, Liu C, Huang J. Light-stimulated synaptic transistors fabricated by a facile solution process based on inorganic perovskite quantum dots and organic semiconductors. *Small*. 2019;15(11):e1900010.
107. Lee YR, Trung TQ, Hwang B-U, Lee N-E. A flexible artificial intrinsic-synaptic tactile sensory organ. *Nat Commun*. 2020;11(1):2753.
108. Tan H, Tao Q, Pande I, et al. Tactile sensory coding and learning with bio-inspired optoelectronic spiking afferent nerves. *Nat Commun*. 2020;11(1):1369. https://doi.org/10.1038/s41467-020-15105-2.
109. Upadhyay NK, Jiang H, Wang Z, Asapu S, Xia Q, Joshua Yang J. Emerging memory devices for neuromorphic computing. *Advanced Materials Technologies*. 2019;4(4):1800589.
110. Yan X, Pei Y, Chen H, et al. Self-assembled networked PbS distribution quantum dots for resistive switching and artificial synapse performance boost of memristors. *Adv Mater*. 2019;31(7):1805284.
111. Li J, Zhang Y, To S, You L, Sun Y. Effect of nanowire number, diameter, and doping density on nano-FET biosensor sensitivity. *ACS Nano*. 2011;5(8):6661–6668.
112. Xue M, Mackin C, Weng W-H, et al. Integrated biosensor platform based on graphene transistor arrays for real-time high-accuracy ion sensing. *Nat Commun*. 2022;13(1):5064.
113. Kim J, Campbell AS, de Ávila BE-F, Wang J. Wearable biosensors for healthcare monitoring. *Nat Biotechnol*. 2019;37(4):389–406.
114. Lin Y, Bariya M, Javey A. Wearable biosensors for body computing. *Adv Funct Mater*. 2021;31(39):2008087.
115. Zhong D, Wu C, Jiang Y, et al. High-speed and large-scale intrinsically stretchable integrated circuits. *Nature*. 2024;627(8003):313–320.
116. Wang T, Wang M, Wang J, et al. A chemically mediated artificial neuron. *Nat. Electron.* 2022;5(9):586–595.
117. Gilhus NE, Verschuuren JJ. Myasthenia gravis: subgroup classification and therapeutic strategies. *Lancet Neurol*. 2015;14(10):1023–1036.
118. Kim D, Lee JS. Neurotransmitter-induced excitatory and inhibitory functions in artificial synapses. *Adv Funct Mater*. 2022;32(21):2200497.
119. Van Doremaele E, Ji X, Rivnay J, Van De Burgt Y. A retrainable neuromorphic biosensor for on-chip learning and classification. *Nat. Electron.* 2023;6(10):765–770.
120. Lim S, Bae J-H, Eum J-H, et al. Adaptive learning rule for hardware-based deep neural networks using electronic synapse devices. *Neural Comput Appl*. 2019;31:8101–8116.
121. Nakata N. Recent technical development of artificial intelligence for diagnostic medical imaging. *Jpn J Radiol*. 2019;37:103–108.
122. Litmanovich D, Bankier AA, Cantin L, Raptopoulos V, Boiselle PM. CT and MRI in diseases of the aorta. *Am J Roentgenol*. 2009;193(4):928–940.
123. Wang Z, Li C, Song W, et al. Reinforcement learning with analogue memristor arrays. *Nature electronics*. 2019;2(3):115–124.
124. Wan W, Kubendran R, Schaefer C, et al. A compute-in-memory chip based on resistive random-access memory. *Nature*. 2022;608(7923):504–512.
125. Zhao H, Liu Z, Tang J, et al. Energy-efficient high-fidelity image reconstruction with memristor arrays for medical diagnosis. *Nat Commun*. 2023;14(1):2276.
126. Tobon-Gomez C, Geers AJ, Peters J, et al. Benchmark for algorithms segmenting the left atrium from 3D CT and MRI datasets. *IEEE Trans Med Imag*. 2015;34(7):1460–1473.
127. Armato IIISG, McLennan G, Bidaut L, et al. The lung image database consortium (LIDC) and image database resource initiative (IDRI): a completed reference database of lung nodules on CT scans. *Med Phys*. 2011;38(2):915–931.
128. Bluethgen C, Chambon P, Delbrouck J-B, et al. A vision–language foundation model for the generation of realistic chest x-ray images. *Nat Biomed Eng*. 2024:1–13.
129. Kim N, Oh J, Kim S, et al. Realistic chest X-ray image synthesis via generative network with stochastic memristor array for machine learning-based medical diagnosis. *Adv Funct Mater*. 2024;34(16):2305136.
130. Wehbe RM, Sheng J, Dutta S, et al. DeepCOVID-XR: an artificial intelligence algorithm to detect COVID-19 on chest radiographs trained and tested on a large US clinical data set. *Radiology*. 2021;299(1):E167–E176.
131. Irvin J, Rajpurkar P, Ko M, et al. *Chexpert: A Large Chest Radiograph Dataset with Uncertainty Labels and Expert Comparison*. 2019:590–597.
132. Cooper RA, Dicianno BE, Brewer B, et al. A perspective on intelligent devices and environments in medical rehabilitation. *Med Eng Phys*. 2008;30(10):1387–1398.
133. Yakub F, Khudzari AZM, Mori Y. Recent trends for practical rehabilitation robotics, current challenges and the future. *Int J Rehabil Res*. 2014;37(1):9–21.
134. Wang W, Jiang Y, Zhong D, et al. Neuromorphic sensorimotor loop embodied by monolithically integrated, low-voltage, soft e-skin. *Science*. 2023;380(6646):735–742.
135. Song K-I, Seo H, Seong D, et al. Adaptive self-healing electronic epineurium for chronic bidirectional neural interfaces. *Nat Commun*. 2020;11(1):4195.
136. Lee Y, Liu Y, Seo D-G, et al. A low-power stretchable neuromorphic nerve with proprioceptive feedback. *Nat Biomed Eng*. 2023;7(4):511–519.
137. Lebedev MA, Nicolelis MA. Brain–machine interfaces: past, present and future. *Trends Neurosci*. 2006;29(9):536–546.
138. Rapeaux AB, Constandinou TG. Implantable brain machine interfaces: first-in-human studies, technology challenges and trends. *Curr Opin Biotechnol*. 2021;72:102–111.
139. Patriarchi T, Cho JR, Merten K, et al. Ultrafast neuronal imaging of dopamine dynamics with designed genetically encoded sensors. *Science*. 2018;360(6396):4422.
140. Da Silva JA, Tecuapetla F, Paixão V, Costa RM. Dopamine neuron activity before action initiation gates and invigorates future movements. *Nature*. 2018;554(7691):244–248.
141. Liu Z, Tang J, Gao B, et al. Neural signal analysis with memristor arrays towards high-efficiency brain–machine interfaces. *Nat Commun*. 2020;11(1):4234.
142. Chaudhary U, Birbaumer N, Ramos-Murguialday A. Brain–computer interfaces for communication and rehabilitation. *Nat Rev Neurol*. 2016;12(9):513–525.
143. Ren H, Li F, Wang M, et al. An ion-mediated spiking chemical neuron based on Mott memristor. *Adv Mater*. 2024;36(33):2403678.
144. Lee JH, Rim YS, Min WK, et al. Biocompatible and biodegradable neuromorphic device based on hyaluronic acid for implantable bioelectronics. *Adv Funct Mater*. 2021;31(50):2107074.
145. Fuentes-Garí M, Velliou E, Misener R, et al. A systematic framework for the design, simulation and optimization of personalized healthcare: making and healing blood. *Comput Chem Eng*. 2015;81:80–93.
146. Williams DF. On the mechanisms of biocompatibility. *Biomaterials*. 2008;29(20):2941–2953.
147. Li T, Chen C, Brozena AH, et al. Developing fibrillated cellulose as a sustainable technological material. *Nature*. 2021;590(7844):47–56.
148. Riecken D. Introduction: personalized views of personalization. *Commun ACM*. 2000;43(8):26–28.